

Reentrant magnetism at the borderline between long-range antiferromagnetic order and spin-glass behavior in the B -site disordered perovskite system $\text{Ca}_{2-x}\text{Sr}_x\text{FeRuO}_6$

Kumari Naveen,¹ Manfred Reehuis,² Peter Adler,^{3,*} Philip Pattison,^{4,5} Andreas Hoser,² Tapas Kumar Mandal,⁶ U. Arjun,⁷ Prashanta K. Mukharjee,⁷ Ramesh Nath,⁷ Claudia Felser,³ and Avijit Kumar Paul^{1,†}

¹Department of Chemistry, National Institute of Technology Kurukshetra, Kurukshetra 136119, India

²Helmholtz-Zentrum Berlin für Materialien und Energie, D-14109 Berlin, Germany

³Max Planck Institute for Chemical Physics of Solids, D-01187 Dresden, Germany

⁴Swiss-Norwegian Beamline, European Synchrotron Radiation Facility, BP 220, F-38042 Grenoble Cedex 9, France

⁵Laboratory for Quantum Magnetism, Swiss Federal Institute of Technology, BSP-Dorigny, CH-1015 Lausanne, Switzerland

⁶Department of Chemistry and Centre of Nanotechnology, Indian Institute of Technology Roorkee, Roorkee 247667, India

⁷School of Physics, Indian Institute of Science Education and Research, Thiruvananthapuram 695551, India



(Received 21 August 2018; published 26 December 2018)

We report on the coexistence of magnetic order and disorder in the atomically disordered double perovskites $\text{Ca}_2\text{FeRuO}_6$ and CaSrFeRuO_6 . Powder x-ray and neutron diffraction were used to investigate the crystal structure and magnetic ordering of these oxides. Both compounds are described by the orthorhombic space group $Pbmn$ down to 3 K, where the B site is found to be statistically occupied by Fe^{3+} and Ru^{5+} ions. The compound $\text{Ca}_2\text{FeRuO}_6$ shows a G -type antiferromagnetic ordering at $T_N \approx 220$ K, where the moments are aligned parallel to the c axis. The exchange of Ca by Sr suppresses long-range ordering in this system with the consequence that CaSrFeRuO_6 shows a diffuse scattering pattern, indicating only the presence of a short-range order of the magnetic moments. Mössbauer measurements additionally reveal the coexistence of a long-range ordered and paramagnetic phase in $\text{Ca}_2\text{FeRuO}_6$, and spin-glass behavior in CaSrFeRuO_6 . The random occupancy of iron and ruthenium atoms at the B site gives rise to locally varying competing magnetic exchange interactions, which favors the emergence of reentrant magnetism with a spin-glass-like transition at $T_f \approx 87$ K for $\text{Ca}_2\text{FeRuO}_6$ and a spin-glass transition at ~ 65 K for CaSrFeRuO_6 , as evidenced by frequency dependent ac susceptibility measurements. Our results are an interesting example for crossing the borderline between antiferromagnetism and spin-glass behavior in a $3d$ - $4d$ hybrid perovskite system by modifying the structural distortion associated to the tolerance factor of the perovskite structure rather than changing the concentration of magnetic ions.

DOI: [10.1103/PhysRevB.98.224423](https://doi.org/10.1103/PhysRevB.98.224423)

I. INTRODUCTION

Perovskite related compounds having the general formula ABO_3 , with diverse combinations of A (alkaline earth or rare-earth metal) and B (transition metal or smaller lanthanide) cations, continue to attract long-term research attention due to their large variety of structural and functional properties [1–10]. Unpaired d electrons of transition metals introduce useful properties such as ferromagnetism, multiferroicity, colossal magnetoresistance, and magnetoimpedance [5–18]. The discovery of colossal tunneling-type magnetoresistance in the $\text{Sr}_2\text{FeMoO}_6$ double perovskite (general formula of double perovskites: $A_2BB'O_6$) also has attracted great attention in solid-state research as this material can be useful for spintronic applications [19]. The combination of two different transition-metal atoms (labeled as B and B') in perovskite related oxides often leads to competing exchange interactions within and between the B and B' sublattices [20–32]. Unusual properties are particularly found due to interactions between strongly correlated $3d$ electrons and less correlated $4d$ or $5d$

electrons, where additionally spin-orbit coupling is considered as essential.

The crystallographic arrangement of different atoms B and B' in the octahedral site strongly influences the structural and physical properties of double perovskites. The degree of atomic order depends on the charge and radius of the B and B' as well as on the A atoms. From earlier reports it is well established that with comparable sizes of B and B' a compound can adopt structure types with disordered cation arrangements at the B site while for a charge difference of more than 2 between them an ordered arrangement of B cations is more likely to be formed [20,29–40]. In order to investigate new double perovskites, the combination of $3d$ transition metals with $4d$ and $5d$ transition metals can be a preferential choice as it combines narrow spin-polarized bands with wider partially filled bands [41]. Previous efforts produced a series of osmium-based double perovskites with unique structural and electronic properties [34–40]. The choice of ruthenium in place of osmium can be fruitful for generating new properties as, while retaining the same number of unpaired d electrons, ruthenium ions have a smaller ionic radius than the corresponding osmium ions and a spin-orbit coupling strength which is intermediate between that of $3d$ and $5d$ ions.

*adler@cpfs.mpg.de

†apaul@nitkkr.ac.in

Due to the substantial itinerant character of the $4d$ electrons, pure ruthenium-based oxides reveal unusual electronic properties at the verge between metallic and insulating behavior [42,43]. A well-studied example presents the Ruddlesden-Popper series $\text{Sr}_{n+1}\text{Ru}_n\text{O}_{3n+1}$. Whereas the $n = \infty$ member SrRuO_3 was the first ferromagnetic $4d$ oxide having an ordering temperature of 160 K [44], the $n = 1$ member Sr_2RuO_4 has attracted a lot of interest as an unconventional superconductor [45,46]. The $n = 2$ member $\text{Sr}_3\text{Ru}_2\text{O}_7$ is a paramagnetic metal with quantum critical behavior [47]. Within the Ruddlesden-Popper series the ruthenium ions are in the $+4$ -oxidation state and the electronic properties evolve from the $4d^4$ (t_{2g}^4) low-spin configuration. The electronic state of ruthenium-based double perovskites, which often contain Ru^{5+} ions (t_{2g}^3 configuration), is more localized and the magnetic states frequently reveal magnetic frustration and glassy characteristics [48–54]. The observation of two-dimensional magnetic correlations and partial long-range magnetic ordering in geometrically frustrated Sr_2YRuO_6 [55] has motivated us to synthesize further magnetically frustrated ruthenium-based compounds and to study their magnetic properties.

Not only the dimensionality of the transition-metal oxide lattice but also cationic substitution at the A site of the perovskite structure is a convenient way for tuning electronic and magnetic properties. If, for instance, the Sr^{2+} ion (ionic radius 1.44 Å for 12-fold coordination) is replaced by the smaller Ca^{2+} (1.34 Å) ion, the tolerance factor t {where $t = (r_A + r_O)/[\sqrt{2}(r_B + r_O)]$, where r_A , r_B , and r_O are the ionic radii of A , B and O , respectively} decreases, which causes large structural distortion with different ground states, strange magnetic ordering, and electronic transitions [48,55–58]. In double perovskites r_B corresponds to the average ionic radius of the B and B' ions. Here, we focus on the system A_2FeRuO_6 . The Sr member, $\text{Sr}_2\text{FeRuO}_6$ [52], as well as phases with minor percentage of Ba and Ca substitution [59], were shown to be atomically disordered spin-glass (SG) systems lacking long-range magnetic order. By contrast, an artificial ordered superlattice of composition $\text{Sr}_2\text{FeRuO}_6$ was reported to be ferro- or ferrimagnetic with T_C as high as 390 K [48]. The behavior of the Ca analog $\text{Ca}_2\text{FeRuO}_6$ and of Ca rich phases in the system $\text{Sr}_{2-x}\text{Ca}_x\text{FeRuO}_6$ is still unknown [20]. The crucial importance of the alkaline-earth ion for tuning the magnetostructural properties of double perovskites was clearly established for the corresponding much more ordered system A_2FeOsO_6 , where a monoclinic crystal structure and ferrimagnetism ($T_C \sim 320$ K) [21], a tetragonal crystal structure and antiferromagnetism ($T_N = 140$ K) [35], and a hexagonal crystal structure with ferrimagnetism ($T_C \sim 370$ K) [60] were found for $A = \text{Ca}$, Sr , and Ba , respectively. In the present paper, we report our systematic study of the crystal structure and magnetic properties of the two B -site disordered perovskites $\text{Ca}_2\text{FeRuO}_6$ (I) and CaSrFeRuO_6 (II). Here, the double perovskite notations were chosen as for the earlier reported compound $\text{Sr}_2\text{FeRuO}_6$ [52] although the transition-metal sites in contrast to the Os analogs are disordered [actually, $\text{CaFe}_{0.5}\text{Ru}_{0.5}\text{O}_3$ (I) and $\text{Ca}_{0.5}\text{Sr}_{0.5}\text{Fe}_{0.5}\text{Ru}_{0.5}\text{O}_3$ (II) in a simple perovskite notation]. Powder x-ray, high-resolution synchrotron, and neutron-diffraction studies were carried out with variation of temperature to investigate the crystal structure and cation

disorder. Neutron-diffraction, Mössbauer, and ac and dc susceptibility measurements were performed to establish the magnetic structures and ordering behavior which reflect competing magnetic exchange interactions. It will be shown that due to the increase in tolerance factor on going from compound I to compound II a change from a long-range ordered antiferromagnetic state with reentrant magnetic behavior to pure spin-glass behavior is induced. The magnetism of the system $\text{Ca}_{2-x}\text{Sr}_x\text{FeRuO}_6$ shows features, which can be compared with those of diluted magnetic systems [61,62] where reentrant magnetism with glassy properties below the magnetic ordering temperature was observed near the percolation threshold. Unusual coexistence of long-range order with spin-glass-like freezing was reported also for several other systems with atomic disorder [63–67].

II. EXPERIMENTAL DETAILS

Synthesis of polycrystalline powders of $\text{Ca}_2\text{FeRuO}_6$ (I) and CaSrFeRuO_6 (II) was carried out by a solid-state method from the stoichiometric ratio of binary oxides. The reagents $\text{CaCO}_3/\text{SrCO}_3$ (Sigma Aldrich, 99%), RuO_2 (Sigma Aldrich, 99.9%), and Fe_2O_3 (Sigma Aldrich, 99%) were used without any further purification. A typical bunch of reagents consisting of a stoichiometric mixture (2:1:0.5) of CaCO_3 , RuO_2 , and Fe_2O_3 for compound I and (1:1:1:0.5) of CaCO_3 , SrCO_3 , RuO_2 , and Fe_2O_3 for compound II was ground for 2 h. After grinding, the powders were pressed into pellets under a pressure of 10 bars. Pressed pellets were first fired at 980 °C for 15 h and then again at 1280 °C for 15 h after intermediate grinding.

At room temperature, powder x-ray-diffraction (PXRD) studies were carried out using a Rigaku diffractometer with a rotating anode $\text{Cu-K}\alpha$ source. The PXRD patterns were collected from 15 to 120° in steps of 0.02° with a counting time of 4 s per step. In order to investigate the structural properties with better accuracy, we have performed high-resolution synchrotron powder-diffraction studies at the beam line BM1A (Swiss-Norwegian) at the ESRF in Grenoble using the x-ray wavelengths $\lambda = 0.6973$ and 0.7152 Å. For this experiment, a powder sample was mounted in a glass capillary of diameter 0.3 mm. A full powder pattern of this sample was collected at 295 K in the 2θ range between 1 and 50°. In the powder patterns, no impurities were found. In order to find possible structural changes in the magnetically ordered state we have collected another powder pattern at 100 K in the 2θ range between 1 and 42°.

dc magnetization (M) was measured as a function of temperature ($2 \leq T \leq 800$ K) and magnetic field ($-9 \leq H \leq +9$ T) using the vibrating sample magnetometer (VSM) attachment to the Physical Property Measurement System (PPMS, Quantum Design). For the high-temperature ($T \geq 400$ K) measurements, a high- T oven was used. ac susceptibility was measured as a function of T and frequency (ν) using the ACMS option of the PPMS. The dc resistivity (ρ) was measured as a function of temperature on a small rectangular pellet in the PPMS using the standard four-probe technique.

Neutron powder-diffraction experiments of both the compounds were carried out on the instruments E6 and E9 at the BER II reactor of the Helmholtz-Zentrum Berlin. The

instrument E9 uses a Ge monochromator selecting the neutron wavelength $\lambda = 1.3087 \text{ \AA}$, while the instrument E6 uses a pyrolytic graphite monochromator selecting the neutron wavelength $\lambda = 2.43 \text{ \AA}$. In order to investigate the crystal structures in detail, low-temperature powder patterns were recorded on the instrument E9 between the diffraction angles 7.5 and 136.5° . The variations of the crystal and magnetic structures of both compounds as a function of temperature were investigated on the instrument E6, where powder patterns were collected between the diffraction angles 5 and 141.8° . Rietveld refinements of the powder-diffraction data were carried out with the program FULLPROF [68]. For the x-ray data we used the atomic scattering factors provided by this program. For the refinement of the neutron powder data, the nuclear scattering lengths $b(\text{O}) = 5.805 \text{ fm}$, $b(\text{Ca}) = 4.70 \text{ fm}$, $b(\text{Fe}) = 9.54 \text{ fm}$, and $b(\text{Ru}) = 7.03 \text{ fm}$ were used [69]. The magnetic form factors of the Fe and Ru atoms were taken from elsewhere [70].

^{57}Fe -Mössbauer spectra were collected between 5.5 and 291 K using a standard WissEl spectrometer operated in the constant acceleration mode ($^{57}\text{Co}/\text{Rh}$ source) and a Janis SHI 850–5 closed cycle refrigerator. The sample powders were mixed with boron nitride and homogeneously distributed in an acrylic glass sample container ($\sim 10 \text{ mg Fe}/\text{cm}^2$). All isomer shifts are given relative to α -iron. The data were evaluated with the MOSSWINN program [71] using the thin absorber approximation.

III. RESULTS AND DISCUSSION

A. Crystal structure

The crystal structures of $\text{Ca}_2\text{FeRuO}_6$ (I) and CaSrFeRuO_6 (II) were investigated by room-temperature laboratory PXRD and high-resolution synchrotron powder diffraction. From the analysis of the powder-diffraction data, it was found that both compounds crystallize in the orthorhombic space group $Pbnm$ (no. 62). The absence of additional Bragg reflections in the diffraction patterns confirms the phase purity of the samples. The shifting of peaks towards lower angles for CaSrFeRuO_6 is due to the incorporation of the larger Sr^{2+} ion at the position of the smaller Ca^{2+} ion in $\text{Ca}_2\text{FeRuO}_6$. An orthorhombic cell is typically observed when the A -O bond length is less than $\sqrt{2}$ times the $(B\text{-O})$ bond length, which results in rotations of the BO_6 octahedra (inset of Fig. 1). It is known that the counterclockwise rotation of equivalent magnitude about the $[0,1,0]$ and $[0,0,1]$ cubic direction and clockwise rotation about $[1,0,0]$ leads to the $Pbnm$ space group. In this space group the Ca atoms in $\text{Ca}_2\text{FeRuO}_6$ occupy the Wyckoff $4c(x,y,1/4)$ positions, whereas Ca and Sr atoms are statistically disordered on $4c(x,y,1/4)$ in CaSrFeRuO_6 as are Fe and Ru on the position $4b(1/2,0,0)$ in both compounds. The O1 and O2 atoms in both compounds I and II fully occupy the Wyckoff positions $4c(x,y,1/4)$ and $8d(x,y,z)$, respectively. The results of the Rietveld analysis of the synchrotron powder data of $\text{Ca}_2\text{FeRuO}_6$ are shown in Fig. 1. The refinement of the positional and isotropic thermal parameters resulted in a residual $R_F = 0.0340$ (defined as $R_F = \sum ||F_{\text{obs}}| - |F_{\text{calc}}|| / \sum |F_{\text{obs}}|$) from the synchrotron data of compound I. In the synchrotron powder-diffraction

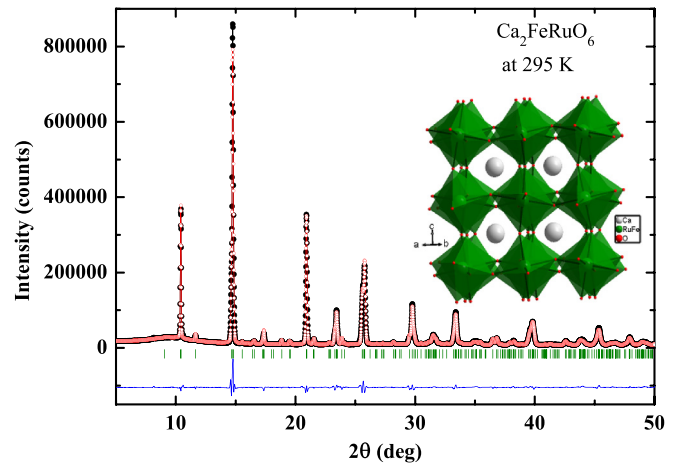


FIG. 1. Results of the Rietveld refinements of the synchrotron powder-diffraction data of $\text{Ca}_2\text{FeRuO}_6$ collected at 295 K with $\lambda = 0.6973 \text{ \AA}$ and refined in the orthorhombic space group $Pbnm$. The calculated patterns (red) are compared with the observed ones (black circles). The difference patterns (blue) as well as the positions (green bars) of the nuclear Bragg reflections are also shown. Inset: Crystal structure of the compound (light gray sphere for Ca, red sphere for O, green octahedra for Fe and Ru).

pattern collected at 100 K , well below the magnetic ordering temperature $T_N \approx 220 \text{ K}$, we could find no evidence of additional peak splitting in the case of $\text{Ca}_2\text{FeRuO}_6$. Further, we could not observe additional Bragg reflections, thus excluding any symmetry lowering. Additionally, laboratory x-ray powder-diffraction data were collected at room temperature for compounds I and II (Figs. S1 and S2 in Supplemental Material [72]), where the refinements resulted in the residuals $R_F = 0.0711$ and 0.0214 , respectively. The results of the refinements are given in Table S1 in Supplemental Material [72]. The resulting bond lengths from powder x-ray data for $\text{Ca}_2\text{FeRuO}_6$ are $d(\text{Fe}/\text{Ru}-\text{O}1) = 1.9541(2) \text{ \AA}$; two O2 distances are $d(\text{Fe}/\text{Ru}-\text{O}2) = 1.9955(10)$ and $1.9831(10) \text{ \AA}$, for CaSrFeRuO_6 $d(\text{Fe}/\text{Ru}-\text{O}1) = 1.9611(2) \text{ \AA}$; two O2 distances are $d(\text{Fe}/\text{Ru}-\text{O}2) = 1.9428(2)$ and $2.0010(1) \text{ \AA}$. These bond lengths are close to those of earlier reported $\text{Sr}_2\text{FeRuO}_6$ [52]. In the present compounds, Fe^{3+} and Ru^{5+} ions exist in $3d^5$ and $4d^3$ configurations with equal ionic radius. An additional confirmation for the oxidation states of Fe and Ru was obtained by bond valence sum (BVS) calculations which were performed by using the room-temperature diffraction data and the SPUDS software. Applying all the possible valence states for Fe and Ru, the best match was found for Fe as Fe^{3+} and Ru as Ru^{5+} oxidation states. Calculated BVS values from powder x-ray data are listed in Table I. The other selected bond lengths and bond angles are also given in Table I.

The crystal structures of compounds I and II were also refined from neutron powder-diffraction data collected on the instrument E9 at 3.2 and 3.0 K , respectively (Fig. 2). Again, the crystal structure could be successfully refined in the space group $Pbnm$ resulting in a residual $R_F = 0.0256$ and 0.0366 for I and II, respectively. In the case of $\text{Ca}_2\text{FeRuO}_6$ some Bragg reflections contained magnetic intensities. The two

TABLE I. Some selected bond lengths, bond angles, and bond valence sums from laboratory PXRD data refinement for (a) $\text{Ca}_2\text{FeRuO}_6$ and (b) CaSrFeRuO_6 , respectively.

(a)			
Bond length	(Å)	Bond angle	(°)
Ca-O1	2.4176(9)	Fe/Ru-O1-Fe/Ru	157.89 (1)
		Fe/Ru-O2-Fe/Ru	150.22 (5)
Ca-O'2	2.6200 (10)	O1-Fe/Ru-O1	180
Ca-O''2	2.6823 (9)	O1-Fe/Ru-O'2	93.49 (2)
Fe/Ru-O1	1.9541 (2)	O1-Fe/Ru-O''2	88.37 (12)
Fe/Ru-O'2	1.9955 (10)	O'2-Fe/Ru-O'2	90.99(4)
Fe/Ru-O''2	1.9831(10)	Fe/Ru-O1-Ca	91.66 (3)
O1-O'2	2.7065 (10)	Fe/Ru-O'2-Ca	85.01 (1)
O1-O''2	2.8234 (10)	Fe/Ru-O''2-Ca	83.58 (2)
O'2-O''2	2.8377 (9)		
BVS calculations			
Fe-O (1) \times 2	1.18	Ru-O (1) \times 2	1.72
	BVS of $\text{Fe}^{3+} = 3.32$		BVS of $\text{Ru}^{5+} = 4.86$
Fe-O' (2) \times 2	1.05	Ru-O' (2) \times 2	1.54
Fe-O'' (2) \times 2	1.09	Ru-O'' (2) \times 2	1.59
(b)			
Bond length	(Å)	Bond angle	(°)
Sr/Ca-O1	2.5873 (1)	Fe/Ru-O1-Fe/Ru	164.40 (1)
		Fe/Ru-O'2-Fe/Ru	160.24 (2)
Sr/Ca-O'2	2.7095 (1)	O1-Fe/Ru-O1	180
Sr/Ca-O''2	2.7198 (2)	O1-Fe/Ru-O'2	90.55 (1)
Fe/Ru-O1	1.9611 (2)	O1-Fe/Ru-O''2	88.27 (1)
Fe/Ru-O'2	1.9428 (2)	O'2-Fe/Ru-O'2	89.58 (2)
Fe/Ru-O''2	2.0010 (1)	Fe/Ru-O1-Ca/Sr	91.15 (1)
O1-O'2	2.8437 (1)	Fe/Ru-O'2-Ca/Sr	87.98 (1)
O1-O''2	2.7470 (1)	Fe/Ru-O''2- Ca/Sr	86.55 (1)
O'2-O''2	2.7992 (2)	Fe/Ru-O1-Fe/Ru	164.40 (1)
		Fe/Ru-O'2-Fe/Ru	160.24 (2)
BVS calculations			
Fe-O (1) \times 2	1.16	Ru-O (1) \times 2	1.70
	BVS of $\text{Fe}^{3+} = 3.40$		BVS of $\text{Ru}^{5+} = 5.00$
Fe-O' (2) \times 2	1.21	Ru-O' (2) \times 2	1.78
Fe-O''(2) \times 2	1.03	Ru-O''(2) \times 2	1.52

strongest reflections are marked in Fig. 2 and the results are summarized in Table II.

B. dc magnetization

The temperature (T) dependent dc susceptibility χ of $\text{Ca}_2\text{FeRuO}_6$ and CaSrFeRuO_6 measured in an applied field of 0.5 T is shown in Figs. 3 and 4, respectively. At higher temperatures, the inverse susceptibility χ^{-1} increases linearly for both compounds with T obeying the Curie-Weiss (CW) law, as expected in the paramagnetic regime. In order to extract the magnetic parameters, $\chi(T)$ in the high- T regime was fitted by the CW law:

$$\chi_{\text{CW}} = \chi_0 + C/(T - \theta). \quad (1)$$

Here χ_0 is the temperature-independent susceptibility, which includes core diamagnetism and Van-Vleck paramagnetism; C is the Curie constant; and θ is the CW temperature. The extracted parameters are tabulated in Table III. The strongly negative value of θ indicates dominant antiferro-

magnetic (AFM) interactions in both the compounds, while the strength of the AFM interactions in $\text{Ca}_2\text{FeRuO}_6$ is much stronger than that in CaSrFeRuO_6 . In both compounds, the expected ionic states of Fe and Ru are Fe^{3+} (d^5 ; $S = 5/2$) and Ru^{5+} (d^3 ; $S = 3/2$), which are having 50% occupancies each in the simple $\text{AFe}_{0.5}\text{Ru}_{0.5}\text{O}_3$ perovskite formula unit. Therefore, the expected effective moment assuming spin-only contributions for both compounds can be calculated as $\mu_{\text{eff}} = \sqrt{0.5 [\mu_{\text{eff}}(\text{Fe}^{3+})]^2 + 0.5 [\mu_{\text{eff}}(\text{Ru}^{5+})]^2} = 5.0 \mu_{\text{B}}$ [using $\mu_{\text{eff}}(\text{Fe}^{3+}) = 5.92 \mu_{\text{B}}$ and $\mu_{\text{eff}}(\text{Ru}^{5+}) = 3.87 \mu_{\text{B}}$]. Thus, our obtained value of μ_{eff} for $\text{Ca}_2\text{FeRuO}_6$ (see Table III) is only slightly smaller than the expected value, which reflects a somewhat reduced Ru^{5+} moment due to spin-orbit coupling and covalency effects. In contrast, the obtained value for CaSrFeRuO_6 is more reduced, which may reflect an insufficient temperature range for the Curie-Weiss analysis (here only measurements up to 400 K were performed).

At lower temperatures, $\text{Ca}_2\text{FeRuO}_6$ shows spontaneous changes in χ near 220 K and below about 90 K, indicating that

TABLE II. Results of the crystal structure refinements of $\text{Ca}_2\text{FeRuO}_6$ and CaSrFeRuO_6 as obtained from synchrotron and neutron powder diffraction. The crystal structure of both compounds was refined in the orthorhombic space group $Pbnm$. The Ca/Sr and O1 atoms occupy Wyckoff $4c(x,y,1/4)$ positions, while the O2 atoms are located at the site $8d(x,y,z)$, respectively. The Fe and Ru atoms are statistically distributed at the site $4b(1/2,0,0)$. The thermal parameters of the oxygen atoms O1 and O2 determined from the neutron data were constrained to be equal during the refinements; for the synchrotron data an overall thermal parameter was used for all atoms.

	$\text{Ca}_2\text{FeRuO}_6$ Synchrotron	$\text{Ca}_2\text{FeRuO}_6$ Neutron	CaSrFeRuO_6 Neutron
T (K)	295	3.2	3.0
Space group	$Pbnm$	$Pbnm$	$Pbnm$
a (Å)	5.40277 (13)	5.3849(4)	5.4790(3)
b (Å)	5.47029 (14)	5.4703(5)	5.4957(4)
c (Å)	7.67262 (19)	7.6520(6)	7.7515(5)
V (Å ³)	226.76 (4)	225.40(3)	233.41(3)
$x(\text{Ca})$	0.9990 (5)	0.9876(13)	0.9981(15)
$y(\text{Ca})$	0.0417 (2)	0.0424(5)	0.0297(5)
$x(\text{O1})$	0.0829 (11)	0.0845(7)	0.0669(10)
$y(\text{O1})$	0.4795 (8)	0.4768(6)	0.4881(9)
$x(\text{O2})$	0.7070 (7)	0.7080(4)	0.7171(6)
$y(\text{O2})$	0.2894 (6)	0.2953(4)	0.2841(6)
$z(\text{O2})$	0.0395 (6)	0.0432(3)	0.0285(4)
$B(\text{Ca/Sr})$ (Å ²)	0.50 (2)	0.51(5)	0.86(10)
$B(\text{Fe/Ru})$ (Å ²)	0.50(2)	0.26(2)	0.50(2)
$B(\text{O})$ (Å ²)	0.50 (2)	0.45(2)	1.03(2)
R_F	0.0340	0.0256	0.0366
$d_{eq}(\text{Fe/Ru-O2})$ (Å)	1.9811(36)	1.9566(24)	1.9631(34)
$d_{eq}(\text{Fe/Ru-O2})$ (Å)	1.9619(35)	1.9913(23)	1.9741(33)
$d_{ap}(\text{Fe/Ru-O1})$ (Å)	1.9729(14)	1.9684(9)	1.9719(11)

the compound undergoes two successive magnetic transitions. In order to confirm these transitions, zero-field cooled (ZFC)

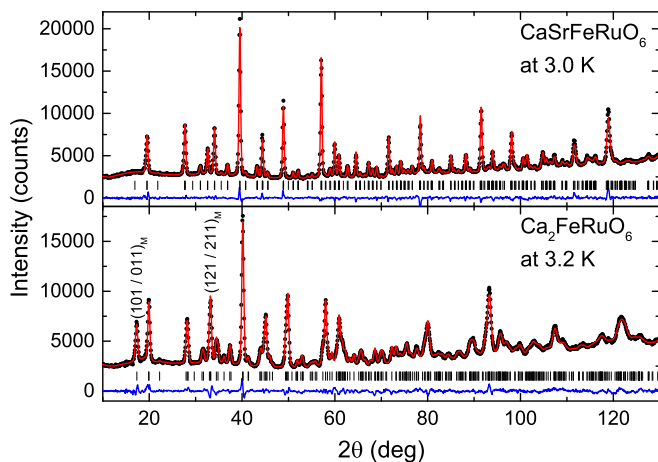


FIG. 2. Results of the Rietveld refinements of the neutron powder-diffraction data of $\text{Ca}_2\text{FeRuO}_6$ and CaSrFeRuO_6 collected at 3.2 and 3.0 K, respectively, on instrument E9 with $\lambda = 1.3087$ Å. The crystal structure of both compounds was refined in the orthorhombic space group $Pbnm$. The calculated patterns (red) are compared with the observed ones (black circles). The difference patterns (blue) as well as the positions (black bars) of the nuclear Bragg reflections are also shown. In the case of $\text{Ca}_2\text{FeRuO}_6$ some Bragg reflection contained magnetic intensities. The two strongest reflections are marked (further details are shown in Fig. 6).

and field cooled (FC) susceptibilities were measured at a very low field of 0.05 T. As shown in the inset of Fig. 3, a clear splitting was observed at 220 K and the ZFC data exhibit two peaks at ~ 220 and ~ 83 K. This further confirms two magnetic transitions. On the other hand, the $\chi(T)$ plot of CaSrFeRuO_6 only shows a single peak at ~ 61 K and the ZFC and FC susceptibilities show a weak splitting at this

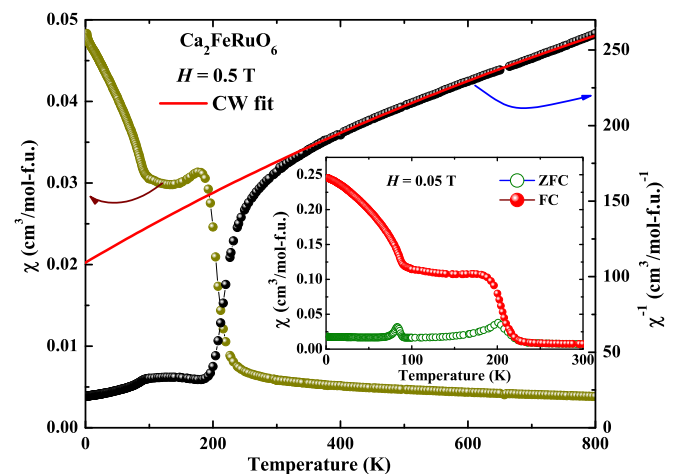


FIG. 3. Magnetic susceptibility $\chi(T)$ of $\text{Ca}_2\text{FeRuO}_6$ measured at $H = 0.5$ T. $1/\chi$ vs T is plotted in the right y axis. The solid line represents the fit using CW law. Inset: ZFC and FC susceptibilities vs T measured at $H = 0.05$ T.

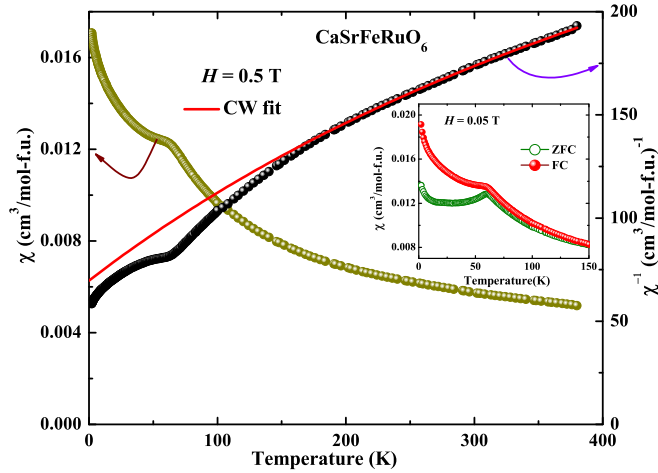


FIG. 4. Magnetic susceptibility $\chi(T)$ of CaSrFeRuO_6 measured at $H = 0.5$ T. $1/\chi$ vs T is plotted in the right y axis. The solid line represents the fit using CW law. Inset: ZFC and FC susceptibilities vs T measured at $H = 0.05$ T.

temperature, which is a possible indication of the occurrence of a SG transition.

Further information on the nature of the magnetic state is obtained from isothermal magnetization data $M(H)$ which were measured at three different temperatures (5, 120, and 320 K) and are shown in Fig. 5. At 320 K, it shows a perfect linear behavior without any hysteresis, as expected in the paramagnetic regime for both the compounds. For $\text{Ca}_2\text{FeRuO}_6$, a hysteresis was observed at $T = 120$ K which is more pronounced at 5 K. On the other hand, for CaSrFeRuO_6 , no hysteresis was observed at 120 K but the data at 5 K show a small hysteresis. The remanent magnetization values of 0.027 and $0.004 \mu_B$ for $\text{Ca}_2\text{FeRuO}_6$ and CaSrFeRuO_6 , respectively, are small and there is no indication of magnetic saturation up to 9 T. These features rule out any ferromagnetic ordering. There is the possibility of a ferrimagnetic ordering since Fe^{3+} and Ru^{5+} carry different moments and an AFM interaction between them can give rise to ferrimagnetism. Such type of peculiar magnetic behavior was reported earlier for osmium-based double perovskites [21,37]. However, our neutron-diffraction experiments (discussed later) could not evidence ferrimagnetic ordering, which is also not expected for the atomically disordered compounds. Thus, the most reasonable explanation of the rise in χ and the hysteresis in the $M(H)$ curve is that $\text{Ca}_2\text{FeRuO}_6$ undergoes an AFM transition at 220 K with slight spin canting giving rise to a ferromagnetic component followed by a SG-like transition near 83 K

TABLE III. Parameters obtained by fitting the high-temperature part of the $\chi^{-1}(T)$ data (380 to 800 K for $\text{Ca}_2\text{FeRuO}_6$ and 290 to 380 K for CaSrFeRuO_6) using the Curie-Weiss law. In our calculation one mol represents the formula units $\text{CaFe}_{0.5}\text{Ru}_{0.5}\text{O}_3$ and $\text{Ca}_{0.5}\text{Sr}_{0.5}\text{Fe}_{0.5}\text{Ru}_{0.5}\text{O}_3$, respectively.

Compounds	χ_0 (cm ³ /mol)	θ (K)	C (cm ³ K/mol)	μ_{eff} (μ_B)
$\text{Ca}_2\text{FeRuO}_6$	0.0014	-370.3	2.87	4.79
CaSrFeRuO_6	0.0020	-166.2	1.75	3.74

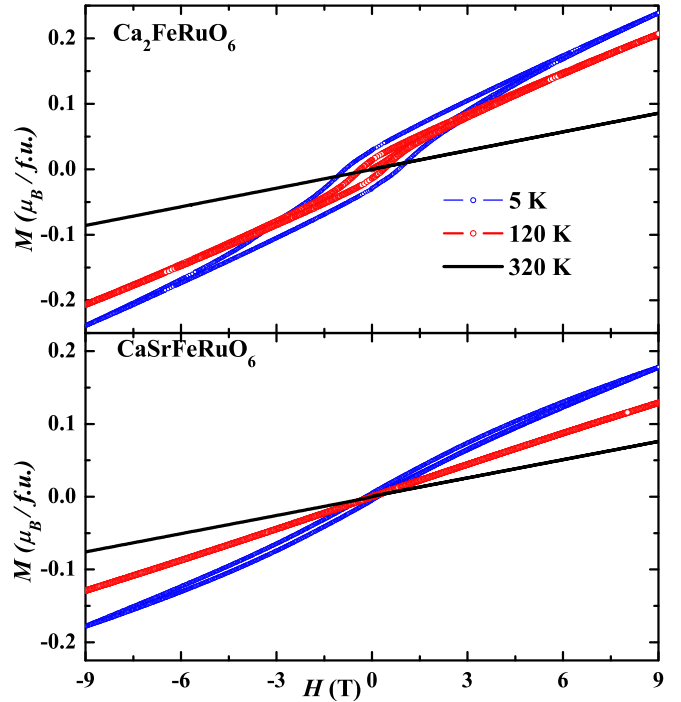


FIG. 5. Isothermal magnetization (M vs H) measured at three different temperatures for $\text{Ca}_2\text{FeRuO}_6$ (upper panel) and CaSrFeRuO_6 (lower panel).

whereas the transition at 61 K observed for CaSrFeRuO_6 is likely to be SG type.

C. Neutron diffraction

In order to investigate the magnetic order of $\text{Ca}_2\text{FeRuO}_6$, we have collected neutron powder patterns on the instrument E6 from 1.6 up to 230 K. In comparison to the data collected at room temperature the strongest magnetic intensity could be observed at the position of the reflection pair 101/011 (Fig. 6). For the Fe and Ru atoms in the position $4b(\frac{1}{2}, 0, 0; \frac{1}{2}, 0, \frac{1}{2}; 0, \frac{1}{2}, 0; 0, \frac{1}{2}, \frac{1}{2})$ magnetic intensity could be generated with a G -type model, where the spin sequence is $+- -+$. In order to determine the moment direction, we carried out Rietveld refinements for different models of spin alignments, where the moments were aligned either parallel to the axis a , or parallel to b or c . Depending on the moment direction one obtains different intensity ratios for the reflections 101 and 011. For μ_x one obtains a ratio of about 1:3, for μ_y one obtains a ratio of 3:1, and for μ_z one obtains a ratio of 1:1. Due to the orthorhombic symmetry the reflections 101 and 011 show a weak splitting of 0.34° , which finally allowed us to find out the correct moment direction. The best fit is obtained when the moment is aligned parallel to the c axis (G_z mode), where the intensity ratio of the reflections 101 and 011 is 1:1.

Possible magnetic structures can be theoretically deduced from Bertaut's representation analysis [73]. Here the four possible spin sequences for the metal atoms in the position $4b$ of the space group $Pbnm$ are labeled $F(++++)$, $G(+ - - +)$, $C(++ - -)$, and $A(+ - + -)$. The analysis shows for the propagation vector $\mathbf{k} = 0$ that a G_z mode can only be admixed with F_x and C_y [representation $\Gamma_2(F_x, C_y, G_z)$

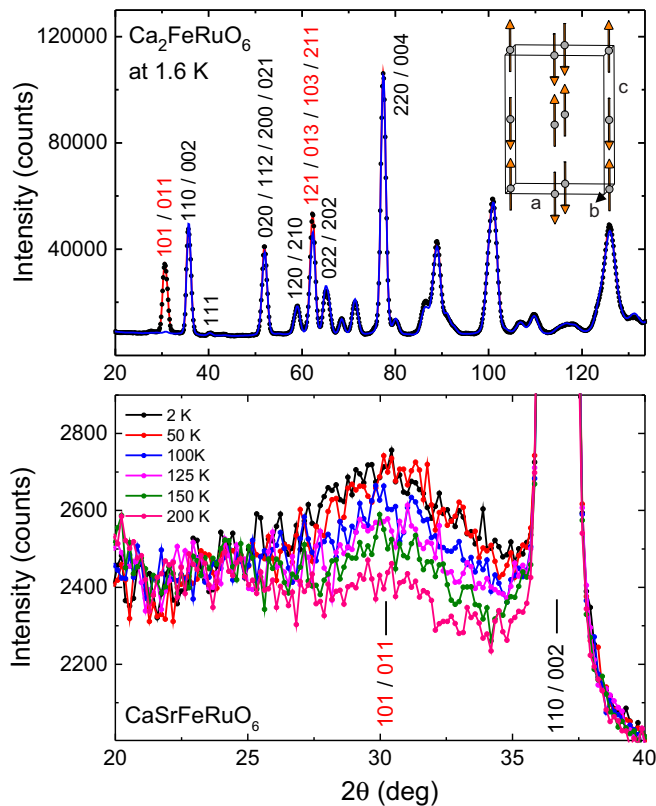


FIG. 6. Neutron powder patterns of $\text{Ca}_2\text{FeRuO}_6$ and CaSrFeRuO_6 taken on instrument E6 with $\lambda = 2.43 \text{ \AA}$. At 1.6 K the strongest magnetic intensity of $\text{Ca}_2\text{FeRuO}_6$ occurs at the positions of the reflection pair 101 and 011 indicating the presence of a G -type spin ordering as shown in the inset of the upper diagram. The calculated pattern of the pure nuclear contribution (blue) as well as the sum of the nuclear and the magnetic contribution (red) is compared with the observed one (black circles). For CaSrFeRuO_6 only a broad diffuse magnetic signal appears below about 150 K close to the position of the reflection pair 101 and 011 indicating a short-range order of the magnetic moments.

or Shubnikov group $Pbn'm'$ given in Table 5 of [Ref. [73]]. Since no magnetic intensity at the position of the reflections at 100, 010, and 001 (forbidden in $Pbnm$) can be detected, the existence of an A - or C -type ordering along the x and y directions is excluded. Interestingly, the magnetization measurements revealed a weak ferromagnetic component. In accordance with the representation analysis a ferromagnetic component should be found along the x direction. Here it has to be mentioned that a weak magnetic component is hardly observable from neutron data, since the weak magnetic signal is superimposed on stronger nuclear reflections. However, a pure G_z -type ordering could be found, for example, for the vanadium moments of YVO_3 [74].

The iron and ruthenium atoms in $\text{Ca}_2\text{FeRuO}_6$ are both located at the Wyckoff position $4b$, hence there is the difficulty to determine their magnetic moments separately. The refinements of the magnetic structure of the Fe/Ru sublattice from the data set collected on E6 resulted in a satisfactory residual $R_M = 0.0359$ (defined as $R_M = \sum ||I_{\text{obs}}| - |I_{\text{calc}}|| / \sum |I_{\text{obs}}|$), where the averaged moment value at 1.6 K is found to

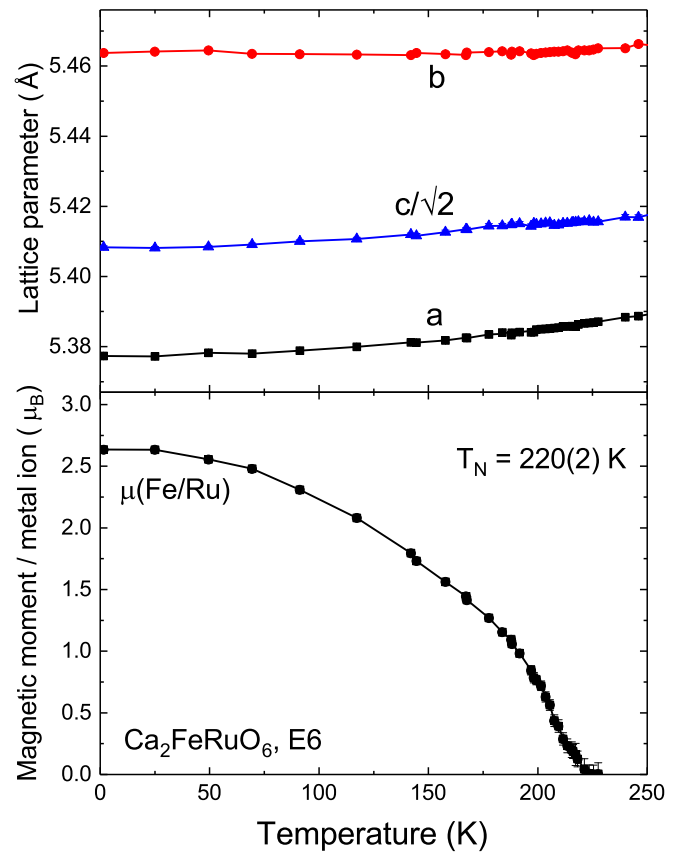


FIG. 7. Temperature dependence of the lattice parameters of $\text{Ca}_2\text{FeRuO}_6$ and the averaged magnetic moment of the transition-metal atoms Fe and Ru at the Wyckoff position $4b$, which is statistically occupied with Fe and Ru atoms.

be $\mu_{\text{exp}}(\text{Fe/Ru}) = 2.63(2) \mu_B$. For comparison, we have obtained from the data set collected on the instrument E9 the moment $\mu_{\text{exp}}(\text{Fe/Ru}) = 2.72(3) \mu_B$ resulting in a residual $R_M = 0.0479$. These values are in good agreement with an average $\mu_{\text{exp}} = 2.75 \mu_B$ which is calculated if we assume a typical value of $\mu_{\text{exp}} = 3.5 \mu_B$ as was obtained for Fe^{3+} ions from neutron data of ternary oxides [35,75,76] and $\mu_{\text{exp}} = 2.0 \mu_B$ for Ru^{5+} ions [77]. This suggests that both Fe^{3+} and Ru^{5+} ions constitute the AFM structure. In contrast to $\text{Ca}_2\text{FeRuO}_6$ we could not find a long-range order in CaSrFeRuO_6 due to the absence of magnetic Bragg reflections. For CaSrFeRuO_6 only a broad diffuse magnetic signal appears below about 150 K (Fig. 6) close to the position of the reflection pair 101/011, where $\text{Ca}_2\text{FeRuO}_6$ showed the strongest magnetic intensity. The appearance of a diffuse peak indicates a short-range order of the magnetic moments.

In the next step, we have investigated the temperature dependence of the lattice parameters for both title compounds and the magnetic moments for $\text{Ca}_2\text{FeRuO}_6$, where the moments of the Fe and Ru atoms are aligned parallel to the c axis. Figure 7 shows that the magnetic moments disappear at about 220 K. Accordingly, the steep rise in the magnetic susceptibility below 220 K seems to correspond to the onset of magnetic ordering. In Fig. 7, we also show the temperature dependence of the lattice parameters. Here one finds no anomaly in the magnetically ordered range. But it can be seen that the lattice

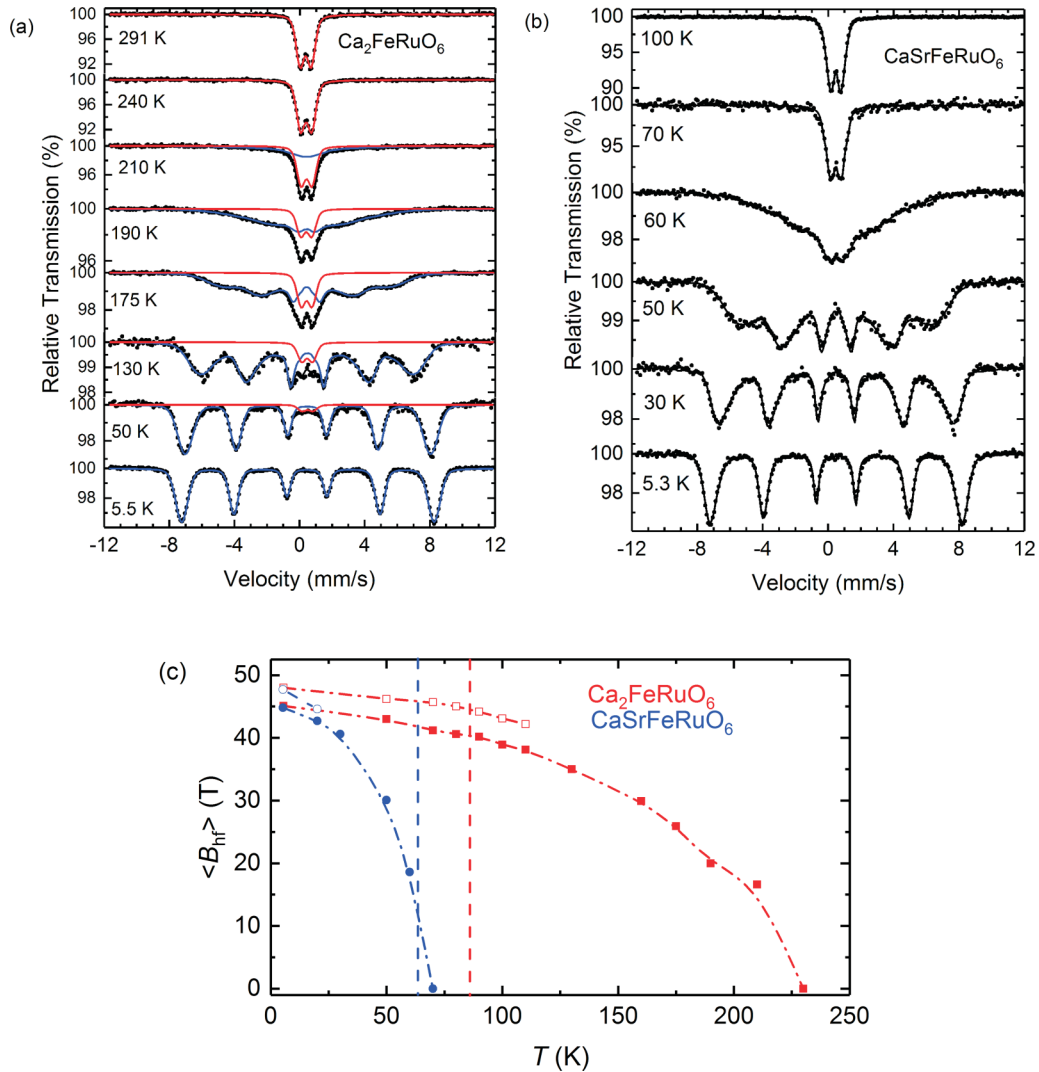


FIG. 8. ^{57}Fe Mössbauer spectra of (a) $\text{Ca}_2\text{FeRuO}_6$ and (b) CaSrFeRuO_6 measured at the indicated temperatures. Dots correspond to the experimental data. Black lines correspond to the calculated spectra. Blue and red lines correspond to the subspectra of the magnetically ordered and paramagnetic component, respectively. (c) Temperature dependence of the average hyperfine field for the two compounds. The vertical red and blue dashed lines correspond to the spin freezing temperatures inferred from the ac susceptibility data of $\text{Ca}_2\text{FeRuO}_6$ and CaSrFeRuO_6 , respectively. Filled symbols correspond to data evaluation using the Hesse-Rübartsch method. Open symbols correspond to data evaluation with a single hyperfine component having a Gaussian B_{hf} distribution. Dash-dotted lines are guides to the eye.

parameters a and c show a slight decrease during the cooling process down to 1.6 K, while the parameter b seems to remain unchanged for $\text{Ca}_2\text{FeRuO}_6$.

D. Mössbauer study

While the neutron-diffraction data reflect the spatially averaged magnetic structure, Mössbauer spectroscopy gives insights into local variations of the magnetic behavior. A set of Mössbauer spectra of $\text{Ca}_2\text{FeRuO}_6$ is shown in Fig. 8(a). For temperatures above 220 K the spectra consist of a broadened quadrupole doublet with an isomer shift (IS) of 0.35 mm/s at 291 K, which is typical for six-coordinated Fe^{3+} in an oxide environment. The line broadening reflects the atomic disorder which leads to a variation in the nearest- and next-nearest-neighbor environment. In order to account for the broadening, the spectra were evaluated assuming a Gaussian distribution

of quadrupole splittings (QS), which leads to average QS of 0.67 mm/s. Both IS and QS are similar as for $\text{Sr}_2\text{FeRuO}_6$ where Fe and Ru are atomically disordered too [52].

Below 220 K magnetic ordering effects are apparent in the spectra. Only at the lowest temperature of 5.5 K all the iron atoms are magnetically ordered (IS = 0.49 mm/s), however due to the atomic disorder the hyperfine pattern is considerably broadened. The spectrum could be best fitted by assuming a Gaussian distribution of hyperfine fields B_{hf} and in addition allowing for a distribution in the quadrupole splitting parameter. The large average B_{hf} of 48 T is typical for $\text{Fe}^{3+}/4d$ or $\text{Fe}^{3+}/5d$ mixed perovskites (cf. $B_{\text{hf}} = 49$ T for $\text{Sr}_2\text{FeRuO}_6$ at 4.2 K [52] and $\text{Sr}_2\text{FeOsO}_6$ at 5 K [35]). With increasing temperature, a paramagnetic contribution occurs in the spectra, the area fraction of which increases continuously with temperature. Even at 50 K a small paramagnetic fraction is discernible. Furthermore, the spectra of the magnetic

component broaden tremendously with increasing temperature and a fit of the spectra with a single Gaussian B_{hf} distribution becomes successively insufficient. In order to reproduce the spectra over the whole temperature range we used the model-independent Hesse-Rübartsch method for extracting the hyperfine field distribution, whereas the paramagnetic component was described by a doublet with a distribution of quadrupole splittings. The average QS and the width of the QS distribution were kept fixed to the values at 240 K, which is above the magnetic ordering temperature. Within this fitting model, any distribution in quadrupole splitting parameters of the magnetic phase is neglected. The isomer shifts of the paramagnetic and magnetically ordered component were constrained to be the same. A magnetic component is seen in the spectra up to 210 K, whereas a spectrum at 230 K consists of a pure quadrupole doublet. Thus, the onset temperature T_m of magnetic order should be between 210 and 230 K, which is in good agreement with the neutron-diffraction data, where $T_m = 220$ K was obtained and with the rise in the susceptibility below 220 K. With increasing temperature, the average hyperfine field decreases gradually from its maximum value [Fig. 8(c)]; a similar behavior is also apparent in the temperature dependence of the magnetic moments (Fig. 7). The broad distributions in B_{hf} [Fig. S3 (top) in Supplemental Material [72]] as well as the coexistence of magnetically ordered and paramagnetic signals over a large temperature range are evidence that the magnetic state is very inhomogeneous. Actually, there is no well-defined magnetic ordering temperature but rather a broad distribution of ordering or freezing temperatures. This can be explained by the variations in the local environment of the Fe^{3+} ions which have a varying number of Fe^{3+} and Ru^{5+} neighbors and thus differing exchange interactions. There are no obvious anomalies in the spectra and parameters near 83 K, where the magnetic susceptibility measurements indicated a further phase transition.

It is instructive to compare the properties of $\text{Ca}_2\text{FeRuO}_6$ with those of the Sr-analog $\text{Sr}_2\text{FeRuO}_6$ [52]. The latter was reported to be a SG system without any evidence of long-range magnetic order. While the low-temperature Mössbauer spectra of $\text{Sr}_2\text{FeRuO}_6$ and $\text{Ca}_2\text{FeRuO}_6$ show similar shapes, a complete collapse of the hyperfine pattern was found for $\text{Sr}_2\text{FeRuO}_6$ near 60 K. By contrast, a magnetic component persists up to 210 K in the spectra of $\text{Ca}_2\text{FeRuO}_6$ and the neutron-diffraction patterns of $\text{Ca}_2\text{FeRuO}_6$ show magnetic Bragg scattering which is supportive of long-range magnetic order. A scenario explaining the broad Mössbauer spectra of $\text{Ca}_2\text{FeRuO}_6$ as well as the quite sluggish magnetic phase transition is to assume the coexistence of long-range magnetic ordered regions with spin or cluster-glass-like regions having smaller magnetic blocking temperatures.

In order to study the evolution of magnetic properties from $\text{Sr}_2\text{FeRuO}_6$ to $\text{Ca}_2\text{FeRuO}_6$ we measured Mössbauer spectra of the intermediate composition CaSrFeRuO_6 [see Fig. 8(b)]. Spectra featuring magnetic hyperfine patterns were evaluated assuming a distribution of magnetic hyperfine fields [Fig. S3 (bottom) in Supplemental Material [72]], while those in the paramagnetic phase were evaluated using a distribution of quadrupole splittings. The distributions were extracted according to the Hesse-Rübartsch method; additionally for the

two lowest temperatures an alternate fit with a single Gaussian distribution in B_{hf} was performed. The temperature dependence of the average B_{hf} is included in Fig. 8(c). The Mössbauer parameters are very similar to those of $\text{Ca}_2\text{FeRuO}_6$: $\text{IS} = 0.37$ mm/s and $\langle \text{QS} \rangle = 0.65$ mm/s at 290 K and $\text{IS} = 0.49$ mm/s and $\langle B_{\text{hf}} \rangle = 48$ T at 5.3 K. It is apparent that the temperature variation of the spectra compares much more with that of $\text{Sr}_2\text{FeRuO}_6$ [52] than with that of $\text{Ca}_2\text{FeRuO}_6$. In particular, there is an inward collapse of the magnetic hyperfine pattern near 60 K, whereas no magnetic components are discernible in spectra for $T \geq 70$ K. These observations are fully consistent with the cusp near 61 K in the $\chi(T)$ data and with the absence of magnetic Bragg reflections in the powder neutron patterns of CaSrFeRuO_6 , which supports the clue that CaSrFeRuO_6 , similar to $\text{Sr}_2\text{FeRuO}_6$, adopts a SG state. Long-range magnetic ordering only occurs for larger Ca contents.

E. ac susceptibility

In order to confirm the SG behavior of the compounds under investigation, ac susceptibility measurements were carried out at different frequencies. The real part of the ac susceptibility χ' as a function of temperature is shown in Fig. 9. As shown in the inset of the upper panel of Fig. 9, $\chi'(T)$ of $\text{Ca}_2\text{FeRuO}_6$ shows a broad peak at around 200 K which is frequency independent, consistent with a canted antiferromagnetic transition observed in the dc magnetization measurements. Another sharp peak was observed at ~ 87 K which is found to be shifted towards higher temperatures and the magnitude of the peak decreases with increasing frequency. These are characteristic features of a SG transition. On the other hand, for CaSrFeRuO_6 , only one transition was observed at ~ 65 K. With increasing frequency, the peak position was found to be shifted towards high temperatures and also the magnitude of the peak decreases, suggesting that the transition is SG type. Thus, $\text{Ca}_2\text{FeRuO}_6$ and CaSrFeRuO_6 undergo SG-type transitions with freezing temperatures $T_f \approx 87$ and 65 K, respectively. To study the spin dynamics, the frequency dependence of the freezing temperature obtained from $\chi'(T)$ was fitted by the conventional power-law divergence of the critical slowing down model [78,79]:

$$\tau = \tau_0[(T_f - T_g)/T_g]^{-z\nu'} . \quad (2)$$

Here τ is the relaxation time corresponding to the measured frequency ($\tau = 1/\nu$), τ_0 is the characteristic relaxation time of a single spin flip, T_g is the SG transition temperature as ν tends to zero, and $z\nu'$ is the dynamic critical exponent. The values of T_g were determined to be ~ 86.6 and ~ 62 K for $\text{Ca}_2\text{FeRuO}_6$ and CaSrFeRuO_6 , respectively, by extrapolating the T_f versus ν plot to $\nu = 0$. The obtained fitting parameters are ($\tau_0 \approx 3.81 \times 10^{-22}$ s and $z\nu' \approx 6.65$) and ($\tau_0 \approx 7.57 \times 10^{-12}$ s and $z\nu' \approx 5.4$) for $\text{Ca}_2\text{FeRuO}_6$ and CaSrFeRuO_6 , respectively. For SG systems, the value of $z\nu'$ typically lies between ~ 4 and 12 while the value of τ_0 ranges from 10^{-10} to 10^{-13} s. Similarly, for the canonical SG and cluster SG, the characteristic range of τ_0 varies from $\sim 10^{-12}$ to $\sim 10^{-13}$ s and $\sim 10^{-7}$ to $\sim 10^{-10}$ s, respectively [80,81]. Our experimental values of $z\nu'$ are consistent with the SG behavior in both the compounds. Similarly, the value of τ_0 for CaSrFeRuO_6

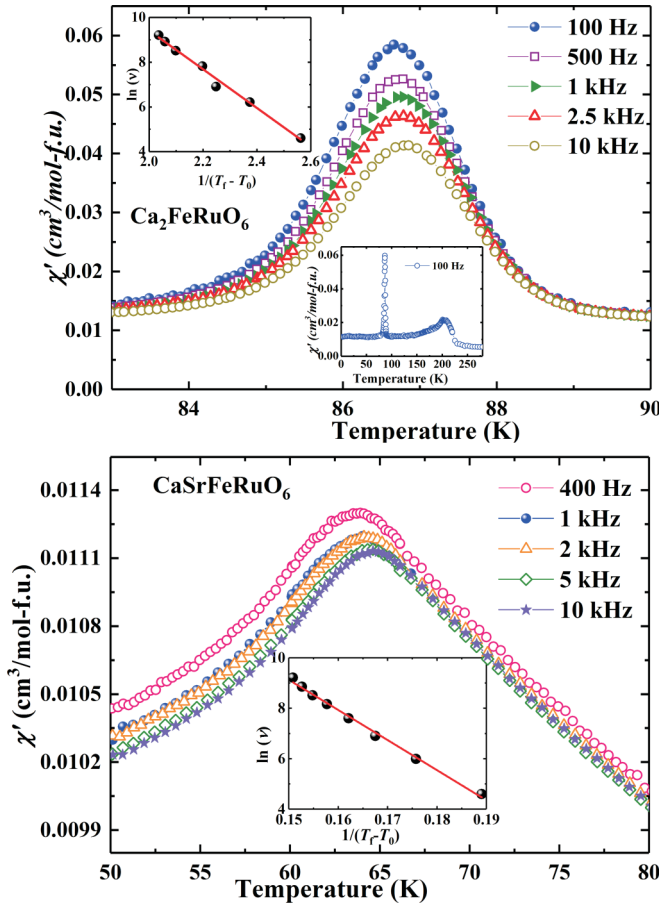


FIG. 9. Upper panel: Real part $\chi'(T)$ of the ac susceptibility of $\text{Ca}_2\text{FeRuO}_6$ measured in an ac field of 8 Oe and at different frequencies. Lower inset: $\chi'(T)$ measured at 100 Hz and for the whole temperature range. Upper inset: Frequency dependence of freezing temperature plotted as $\ln(\nu)$ vs $1/(T_f - T_0)$ together with the fit using the Vogel-Fulcher law. Lower panel: $\chi'(T)$ of CaSrFeRuO_6 measured in an ac field of 8 Oe and at different frequencies. Inset: $\ln(\nu)$ vs $1/(T_f - T_0)$ together with the fit using Vogel-Fulcher law.

falls in the range corresponding to the canonical SG. On the other hand, for $\text{Ca}_2\text{FeRuO}_6$ the value of τ_0 is found to be unphysically small.

In order to estimate the activation energy, we tried to fit the frequency dependence of T_f by the simple Arrhenius law, which does not give a good fit, suggesting that the dynamics is not simply associated with single spin flips but rather reflects a cooperative character of the freezing-in process in both the compounds. However, the frequency dependence of T_f could be fitted well using the Vogel-Fulcher law [79]:

$$\nu = \nu_0 \exp[-E_a/k_B(T_f - T_0)], \quad (3)$$

where ν_0 is the characteristic attempt frequency, E_a is the activation energy, and T_0 is the Vogel-Fulcher temperature, which is often interpreted as a measure of the effective interaction between spins or clusters. The fits are shown in the insets of Fig. 9. The obtained best fit parameters are ($\nu_0 \approx 4.06 \times 10^{11} \text{ s}^{-1}$, $T_0 \approx 86.3 \text{ K}$, and $E_a/k_B \approx 8.6 \text{ K}$) for $\text{Ca}_2\text{FeRuO}_6$ and ($\nu_0 \approx 5.4 \times 10^{11} \text{ s}^{-1}$, $T_0 \approx 58 \text{ K}$, and $E_a/k_B \approx 119 \text{ K}$) for CaSrFeRuO_6 . The estimated values of ν_0 in both the

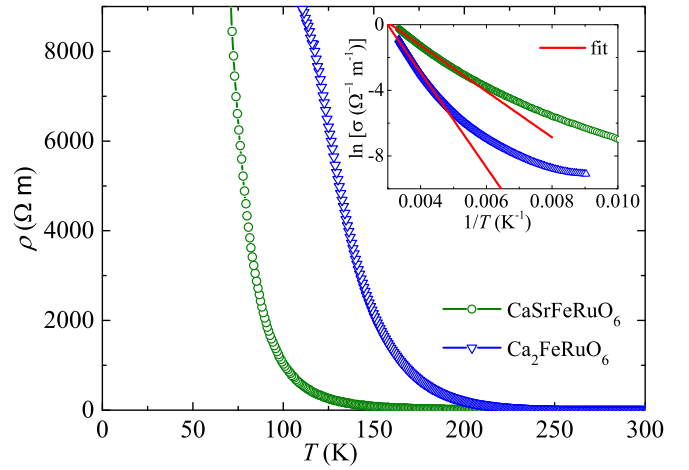


FIG. 10. The electrical resistivity $\rho(T)$ of $\text{Ca}_2\text{FeRuO}_6$ and CaSrFeRuO_6 measured at zero field. Inset: $\ln(\sigma)$ vs $1/T$. The solid lines are the fits to the data using Eq. (4).

compounds are in the intermediate range expected for canonical and cluster SG systems [82]. Moreover, the development of a glassy phase below a magnetically ordered phase is commonly referred to as “reentrant SG [61].” In $\text{Ca}_2\text{FeRuO}_6$, the canted antiferromagnetic transition at high temperatures is followed by a low-temperature SG transition, thus reflecting reentrant-SG behavior.

F. Resistivity

The temperature-dependent electrical resistivity $\rho(T)$ of $\text{Ca}_2\text{FeRuO}_6$ and CaSrFeRuO_6 was measured at zero field as shown in Fig. 10. For both the compounds, $\rho(T)$ increases rapidly with decreasing T , suggesting insulating ground states. At low temperatures the resistances could not be measured since the resistance values exceeded the instrument’s measurement limit. The conductivity data ($\sigma = \frac{1}{\rho}$) in the high-temperature regime were fitted using a law for activated transport:

$$\sigma(T) = A \exp\left(\frac{-\Delta}{k_B T}\right), \quad (4)$$

where Δ is the activation energy, k_B is the Boltzmann constant, and A is the proportionality constant. The inset of Fig. 10 shows the plot of $\ln(\sigma)$ versus $1/T$ to highlight the approximately linear behavior in the high-temperature regime. Our fit in the temperature range $217 \leq T \leq 300 \text{ K}$ for $\text{Ca}_2\text{FeRuO}_6$ and $188 \leq T \leq 300 \text{ K}$ for CaSrFeRuO_6 yields $\Delta \approx 0.25 \text{ eV}$ and $\approx 0.12 \text{ eV}$, respectively. Thus, Sr^{2+} substitution at the Ca^{2+} site leads to a reduction of band gap and increase in conductivity.

It is interesting to note that the $\ln(\sigma)$ versus $1/T$ plots show an approximately linear behavior only in the high-temperature regime. However, a linearity over an extended temperature range, in particular for CaSrFeRuO_6 , was obtained when $\ln(\sigma)$ was plotted against $(1/T)^{1/4}$ (Fig. S4 in Supplemental Material [72]) which possibly suggests that a three-dimensional variable range hopping (VRH) transport mechanism [83,84] proposed by Mott and Davis is operative

in these two systems. The VRH mechanism normally occurs in the low-temperature region (below room temperature) where the energy is insufficient to excite the charge carriers across the Coulomb gap. This type of behavior was reported in various double perovskites and related materials [20,85–87].

G. Magnetism in $\text{Ca}_{2-x}\text{Sr}_x\text{FeRuO}_6$: Summarizing discussion

Atomically ordered as well as disordered $A_2BB'O_6$ perovskites are a versatile playground for magnetism and a large variety of magnetic properties has been realized in this class of compounds [20]. This is a consequence of the chemical flexibility of perovskites and of the various exchange pathways in $A_2BB'O_6$ systems with magnetic B and B' ions which often lead to competing exchange interactions and signatures of magnetic frustration. The balance of interactions and in some cases even the type of magnetic order depends on the size of the A cation. A large degree of magnetic frustration particularly may occur in atomically disordered compounds where the atomic disorder together with competing exchange pathways in several cases leads to spin-glass behavior. Examples related to the present $\text{Ca}_{2-x}\text{Sr}_x\text{FeRuO}_6$ system are the compounds $\text{Sr}_2\text{Fe}B'\text{O}_6$ with $B' = \text{Nb}$ and Ta [20]. Also the previously reported $\text{Sr}_2\text{FeRuO}_6$ [52] is such a spin-glass system. Here, we replaced the larger Sr^{2+} by smaller Ca^{2+} ions, which decreases the tolerance factor and in turn enhances the degree of tilting of the octahedra in the perovskite structure. This leads to a drastic change in the magnetic properties: In contrast to $\text{Sr}_2\text{FeRuO}_6$ we observed long-range antiferromagnetic order below $T_N = 220$ K with the peculiarity of reentrant spin-glass behavior at lower temperatures (87 K) for $\text{Ca}_2\text{FeRuO}_6$ (I). Slight enhancement of the tolerance factor from 0.969 (I) to 0.987 in CaSrFeRuO_6 (II) is sufficient to suppress the long-range magnetic order and similar to $\text{Sr}_2\text{FeRuO}_6$ spin-glass behavior was observed. Both compounds have insulating ground states, but the activation energy for the charge transport in compound II is smaller than in compound I, which is in line with the smaller structural distortion in compound II.

The magnetic features of the present system are reminiscent of comparable phenomena in other systems featuring atomic and magnetic disorder, e.g., metallic ferromagnetic alloy systems like AuFe [61] or the ferrimagnetic spinel system $\text{Mg}_{1+x}\text{Fe}_{2-2x}\text{Ti}_x\text{O}_4$ [62]. In these cases, the concentration c of magnetic ions was changed systematically and it was shown that a reentrant magnetic state occurs near the percolation threshold c_p , where the system changes from long-range magnetic order to spin-glass behavior. By contrast, in the present system $\text{Ca}_{2-x}\text{Sr}_x\text{FeRuO}_6$ the concentration of magnetic ions remains unchanged. However, due to the change in tolerance factor the strength of exchange interactions and thus the temperature at which cooperative magnetic ordering occurs is changed because the exchange interactions strongly vary with bond angles. For instance, in compound I, the Fe/Ru-O1-Fe/Ru bond angle along the z axis is 157.9° , which is lower (164.4°) than the observed Fe/Ru-O1-Fe/Ru bond angle of compound II. The Fe/Ru-O2-Fe/Ru bond angle along the xy plane is also lower in compound I (150.2°) than in compound II (160.2°). In the case of the related atomically ordered Os^{5+} double perovskite system $\text{Ca}_{2-x}\text{Sr}_x\text{FeOsO}_6$, the different magnetic structures of $\text{Ca}_2\text{FeOsO}_6$ and $\text{Sr}_2\text{FeOsO}_6$

(ferrimagnetic and antiferromagnetic, respectively) were attributed to the strengthening of the ferromagnetic σ -exchange pathway between Fe^{3+} and Os^{5+} ions with respect to the antiferromagnetic π -exchange pathway as the Sr content increases [88,89]. This reflects the pronounced magnetostructural correlations where the ferromagnetic pathway is favored for a smaller deviation of the Fe-O-Os bond angle from 180° . Since Ru^{5+} and Os^{5+} ions both have d^3 electron configurations similar arguments apply for the present system. It is noted that according to the Goodenough-Kanamori rule ferromagnetic coupling is expected in the case of d^3 - d^5 high-spin interactions, but due to the higher energy of the unoccupied e_g levels of $4d^3$ and $5d^3$ systems the ferromagnetic exchange path is weakened compared to $3d^3$ systems. Furthermore, due to the atomic disorder in compounds I and II the balance of nearest-neighbor and next-nearest-neighbor exchange interactions is even more complicated. For instance, not only Fe^{3+} - Ru^{5+} but also antiferromagnetic Fe^{3+} - Fe^{3+} and Ru^{5+} - Ru^{5+} nearest-neighbor interactions have to be taken into account. In such a situation of competing interactions it is easily conceivable that subtle structural modifications which change the balance of interactions lead to frustration and spin-glass behavior. The sensitive dependence of the coherence of the spin system on the detailed balance of exchange interactions has been demonstrated for $\text{Sr}_2\text{FeRuO}_6$ by Monte Carlo simulations [90]. In any case, from the Curie-Weiss temperatures (Table III) and the observation of long-range magnetic order it can be concluded that the average AFM interactions are dominating in the more distorted $\text{Ca}_2\text{FeRuO}_6$ and their strength decreases with increasing Sr content. This corroborates the trend already seen in lightly Ca-substituted samples of $\text{Sr}_2\text{FeRuO}_6$ [59]. The occurrence of long-range ordering with a quite large T_N of 220 K is reflected in a small frustration factor $f = |\theta|/T_N = 1.7$, whereas strong frustration effects are typically indicated by $f > 10$ [20]. Nevertheless, in the calcium rich regime the $\text{Ca}_{2-x}\text{Sr}_x\text{FeRuO}_6$ system appears to be at the borderline between long-range antiferromagnetic order and spin-glass behavior. In this situation, reentrant magnetism with long-range ordering below T_N and additional spin freezing below $T_f < T_N$ is observed, while for increased Sr contents atomic disorder and competing exchange interactions drive the system towards a pure spin glass. A comparable reentrant state as in $\text{Ca}_2\text{FeRuO}_6$ was reported for the disordered perovskites $\text{PbFe}_{0.5}\text{Nb}_{0.5}\text{O}_3$ [63] and $\text{PbFe}_{0.5}\text{Ta}_{0.5}\text{O}_3$ [64] ($\text{Pb}_2\text{FeNbO}_6$ and $\text{Pb}_2\text{FeTaO}_6$ in our notation).

For explaining the reentrant magnetism two scenarios may be considered. The first one corresponds to microscopic phase separation where large (“infinite”) clusters revealing long-range order coexist with smaller clusters remaining paramagnetic above a freezing temperature $T_f < T_N$ [65,91]. In this case, the 87-K transition would correspond to the freezing of such smaller clusters. In fact, the Mössbauer spectra of $\text{Ca}_2\text{FeRuO}_6$ verify the coexistence of paramagnetic and magnetically ordered regions over a large temperature range and thus suggest the presence of clusters with smaller ordering temperatures, in contrast to the disordered perovskite systems in Refs. [63,64], where no such clusters were observed. The origin of this difference may be a more complicated balance of exchange interactions as the Ru^{5+} ions are magnetic whereas the Nb^{5+} and Ta^{5+} ions are nonmagnetic. Clustering may

be a signature of partial cation ordering as, for instance, in $\text{Sr}_2\text{FeSbO}_6$ [20] but there is no experimental evidence for this in the present paper. Obviously, there is no correlation between the appearance of the paramagnetic signal in the Mössbauer spectra and the T_f obtained from the dc and ac susceptibility measurements. The paramagnetic signal increases gradually with temperature and the broad hyperfine patterns rather suggest a distribution of freezing temperatures and thus of cluster sizes which is difficult to reconcile with the sharp freezing temperature of 87 K. Another scenario which was favored to explain the reentrant magnetic properties in the above-mentioned systems [61–63,92] is that below T_N long-range magnetic order occurs along the z direction, whereas the transverse moments remain magnetically disordered and freeze below $T_f < T_N$. In such a model the anomaly in the ac and dc susceptibilities of $\text{Ca}_2\text{FeRuO}_6$ would correspond to the freezing of the transverse magnetic moments. This would naturally explain the well-defined transition temperature and the coexistence of the long-range magnetic order with spin-glass-like features. In this scenario the spin freezing is an intrinsic property of the material giving rise to spin canting, and not a consequence of phase separation. In several magnetically diluted reentrant systems the additional spin freezing is reflected in an anomaly in the temperature dependence of the Mössbauer hyperfine field [61–63,92], but such an anomaly is not apparent in the B_{hf} data of $\text{Ca}_2\text{FeRuO}_6$ [Fig. 8(c)]. The present system may involve both cluster formation and transverse spin freezing but this issue cannot be resolved unambiguously from the present data.

IV. CONCLUSION

In summary, two $3d$ - $4d$ hybrid double perovskites $\text{Ca}_2\text{FeRuO}_6$ and CaSrFeRuO_6 have been synthesized at ambient pressure and characterized using a combination of different techniques in order to study the nature of glassy

features in their magnetic properties. Both compounds crystallize in the orthorhombic centrosymmetric space group $Pbnm$, where the B site is randomly occupied by Fe^{3+} and Ru^{5+} ions in the $4b$ position. Although $\text{Ca}_2\text{FeRuO}_6$ shows G -type antiferromagnetic ordering below 220 K, competition between the various exchange interactions due to atomic disorder causes reentrant magnetic behavior with glassy spin freezing at 87 K as evidenced by the frequency dependence of ac susceptibility. Substitution of Ca by Sr in A position leads to the formation of a conventional spin-glass system by destroying long-range ordering. By varying the composition at the A sites, the balance of competing superexchange pathways between the transition metals in B and B' position is modified which induces a change from long-range ordering to spin-glass behavior. In this crossover region reentrant magnetism is observed, similar as in diluted magnetic systems where crossover between spin-glass behavior and long-range order occurs near the percolation threshold. Here, rather a critical tolerance factor t_c separating the magnetic regimes may be defined. The system $\text{Ca}_{2-x}\text{Sr}_x\text{FeRuO}_6$ is an interesting model case for studying the transition region between a spin glass and magnetic order in undiluted mixed perovskites with competing exchange interactions. Further investigations in the Ca-rich region are required to establish more details of the magnetic phase diagram.

ACKNOWLEDGMENTS

The authors thank the Department of Science and Technology, Government of India, for an INSPIRE Faculty Award (Grant No. IFA14-CH-144). The Science and Engineering Research Board (SERB), Government of India, is also thanked for the award of a Fast Track startup grant (Grant No. SB/FT/CS-098/2014). This research was supported in part by SERB.

-
- [1] J. R. Petrie, V. R. Cooper, J. W. Freeland, T. L. Meyer, Z. Zhang, D. A. Lutterman, and H. N. Lee, Enhanced bifunctional oxygen catalysis in strained LaNiO_3 perovskites, *J. Am. Chem. Soc.* **138**, 2488 (2016).
 - [2] M.-G. Ju, J. Dai, L. Ma, and X. C. Zeng, Lead-free mixed tin and germanium perovskites for photovoltaic application, *J. Am. Chem. Soc.* **139**, 8038 (2017).
 - [3] Y. Hosaka, N. Ichikawa, T. Saito, P. Manuel, D. Khalyavin, J. P. Attfield, and Y. Shimakawa, Two-dimensional charge disproportionation of the unusual high valence state Fe^{4+} in a layered double perovskite, *J. Am. Chem. Soc.* **137**, 7468 (2015).
 - [4] J. K. Burdett and G. V. Kulkarni, Defect patterns in perovskites, *J. Am. Chem. Soc.* **110**, 5361 (1988).
 - [5] W. Fang, C. Zhang, F. Steinbach, and A. Feldhoff, Stabilizing perovskite structure by interdiffusional tailoring and its application in composite mixed oxygen-ionic and electronic conductors, *Angew. Chem. Int. Ed.* **56**, 7584 (2017).
 - [6] D. G. Lee, O. Gwon, H. S. Park, S. H. Kim, J. Yang, S. K. Kwak, G. Kim, and H. K. Song, Conductivity-dependent completion of oxygen reduction on oxide catalysts, *Angew. Chem. Int. Ed.* **54**, 15730 (2015).
 - [7] M. R. Li, M. Retuerto, D. Walker, T. Sarkar, P. W. Stephens, S. Mukherjee, T. S. Dasgupta, J. P. Hodges, M. Croft, and C. P. Grams, Magnetic-structure-stabilized polarization in an above-room-temperature ferrimagnet, *Angew. Chem. Int. Ed.* **53**, 10774 (2014).
 - [8] H. Seki, Y. Hosaka, T. Saito, M. Mizumaki, and Y. Shimakawa, Ferromagnetism induced by substitution of the iron (IV) ion by an unusual high-valence nickel (IV) ion in antiferromagnetic SrFeO_3 , *Angew. Chem. Int. Ed.* **55**, 1360 (2016).
 - [9] W. Si, Y. Wang, Y. Peng, and J. Li, Selective dissolution of A -site cations in ABO_3 perovskites: A new path to high-performance catalysts, *Angew. Chem. Int. Ed.* **54**, 7954 (2015).
 - [10] L. Zhu, Y. Liu, C. Su, W. Zhou, M. Liu, and Z. Shao, Perovskite $\text{SrCo}_{0.9}\text{Nb}_{0.1}\text{O}_{3-\delta}$ as an anion-intercalated electrode material for supercapacitors with ultrahigh volumetric energy density, *Angew. Chem. Int. Ed.* **55**, 9576 (2016).
 - [11] J. Santamaría, Interfaces on stage, *Nat. Phys.* **2**, 229 (2006).
 - [12] J. Mannhart and D. G. Schlom, Oxide interfaces: An opportunity for electronics, *Science* **327**, 1607 (2010).
 - [13] E. Dagotta, When oxides meet face to face, *Science* **318**, 1076 (2007).

- [14] Y. Zhu, W. Zhou, Z. G. Chen, Y. Chen, C. Su, M. O. Tadé, and Z. Shao, SrNb_{0.1}Co_{0.7}Fe_{0.2}O_{3- δ} perovskite as a next-generation electrocatalyst for oxygen evolution in alkaline solution, *Angew. Chem. Int. Ed.* **54**, 3897 (2015).
- [15] H. Xu, B. Chen, F. Jin, Z. Guo, G. Gao, F. Chen, and W. Wu, Enhanced conductivity and metal-insulator transition of ultrathin CaRuO₃ in superlattices, *Mater. Res. Express* **3**, 126403 (2016).
- [16] J. Gunasekera, L. Harrige, A. Dahal, T. Heitmann, G. Vignale, and D. K. Singh, Magnetic fluctuations driven insulator-to-metal transition in Ca(Ir_{1-x}Ru_x)O₃, *Sci. Rep.* **5**, 18047 (2015).
- [17] H. J. Zhao, L. Bellaiche, X. M. Chen, and J. Iniguez, Improper electric polarization in simple perovskite oxides with two magnetic sublattices, *Nat. Commun.* **8**, 14025 (2017).
- [18] J. Deng, M. A. Farid, M. Zhang, A. Yang, H. Zhang, G. Tian, W. Wu, L. Liu, J. Sun, G. Li, F. Liao, and J. Lin, Enhancement of ferroelectricity for orthorhombic (Tb_{0.861}Mn_{0.121})MnO_{3- δ} by copper doping, *Inorg. Chem.* **56**, 3475 (2017).
- [19] K.-I. Kobayashi, T. Kimura, H. Sawada, K. Terakura, and Y. Tokura, Room-temperature magnetoresistance in an oxide material with an ordered double-perovskite structure, *Nature (London)* **395**, 677 (1998).
- [20] S. Vasala and M. Karppinen, A₂B'B''O₆ perovskites: A review, *Prog. Solid State Chem.* **43**, 1 (2015).
- [21] H. L. Feng, M. Arai, Y. Matsushita, Y. Tsujimoto, Y. Guo, C. I. Sathish, X. Wang, Y.-H. Yuan, M. Tanaka, and K. Yamaura, High-temperature ferrimagnetism driven by lattice distortion in double perovskite Ca₂FeOsO₆, *J. Am. Chem. Soc.* **136**, 3326 (2014).
- [22] R. Pradheesh, H. S. Nair, C. M. N. Kumar, J. Lamsal, R. Nirmala, P. N. Santhosh, W. B. Yelon, S. K. Malik, V. Sankaranarayanan, and K. Sethupathi, Observation of spin glass state in weakly ferromagnetic Sr₂FeCoO₆ double perovskite, *J. Appl. Phys.* **111**, 053905 (2012).
- [23] M. A. de Vries, A. C. McLaughlin, and J.-W. G. Bos, Valence Bond Glass on an Fcc Lattice in the Double Perovskite Ba₂YMoO₆, *Phys. Rev. Lett.* **104**, 177202 (2010).
- [24] D. Serrate, J. M. Da Teresa, and M. R. Ibarra, Magnetoelastic coupling in Sr₂(Fe_{1-x}Cr_x)ReO₆ double perovskites, *J. Phys.: Condens. Matter.* **19**, 023201 (2007).
- [25] T. K. Mandal and J. Gopalakrishnan, New route to ordered double perovskites: Synthesis of rock salt oxides, Li₄MWO₆, and their transformation to Sr₂MWO₆ (M = Mg, Mn, Fe, Ni) via metathesis, *Chem. Mater.* **17**, 2310 (2005); A. Nag, J. Manjanna, R. M. Tiwari, and J. Gopalakrishnan, Sr₄M₃ReO₁₂ (M = Co, Fe): New ferromagnetic perovskite oxides, *ibid.* **20**, 4420 (2008).
- [26] R. I. Dass, J.-Q. Yan, and J. B. Goodenough, Ruthenium double perovskites: Transport and magnetic properties, *Phys. Rev. B* **69**, 094416 (2004).
- [27] H. Gao, A. Liobet, J. Barth, J. Winterlik, C. Felser, M. Panthöfer, and W. Tremel, Structure-property relations in the distorted ordered double perovskite Sr₂InReO₆, *Phys. Rev. B* **83**, 134406 (2011).
- [28] C. Felser, G. H. Fecher, and B. Balke, Spintronics: A challenge for materials science and solid-state chemistry, *Angew. Chem. Int. Ed.* **46**, 668 (2007).
- [29] O. N. Meetei, O. Erten, M. Randeria, N. Trivedi, and P. Woodward, Theory of High T_C Ferrimagnetism in a Multiorbital Mott Insulator, *Phys. Rev. Lett.* **110**, 087203 (2013).
- [30] T. K. Mandal, C. Felser, M. Greenblatt, and J. Kubler, Magnetic and electronic properties of double perovskites and estimation of their Curie temperatures by *ab initio* calculations, *Phys. Rev. B* **78**, 134431 (2008).
- [31] Y. Krockenberger, K. Mogare, M. Reehuis, M. Tovar, M. Jansen, G. Vaitheeswaran, V. Kanchana, F. Bultmark, A. Delin, F. Wilhelm, A. Rogalev, A. Winkler, and L. Alff, Sr₂CrOsO₆: End point of a spin-polarized metal-insulator transition by 5d band filling, *Phys. Rev. B* **75**, 020404(R) (2007); Y. Krockenberger, M. Reehuis, M. Tovar, K. Mogare, M. Jansen, and L. Alff, A neutron scattering study of the crystal and magnetic structure of Sr₂CrOsO₆, *J. Magn. Magn. Mater.* **310**, 1854 (2007).
- [32] M. Retuerto, F. Jimenez-Villacorta, M. J. Martinez-Lope, Y. Huttel, E. Roman, M. T. Fernandez-Diaz, and J. A. Alonso, Study of the valence state and electronic structure in Sr₂FeMO₆ (M = W, Mo, Re and Sb) double perovskites, *Phys. Chem. Chem. Phys.* **12**, 13616 (2010).
- [33] R. Morrow, R. Mishra, O. D. Restrepo, M. R. Ball, W. Windl, S. Wurmehl, U. Stocker, B. Buechner, and P. M. Woodward, Independent ordering of two interpenetrating magnetic sublattices in the double perovskite Sr₂CoOsO₆, *J. Am. Chem. Soc.* **135**, 18824 (2013).
- [34] B. Yan, A. K. Paul, S. Kanungo, M. Reehuis, A. Hoser, D. M. Többens, W. Schnelle, R. C. Williams, T. Lancaster, F. Xiao, J. S. Möller, S. J. Blundell, W. Hayes, C. Felser, and M. Jansen, Lattice-Site-Specific Spin Dynamics in Double Perovskite Sr₂CoOsO₆, *Phys. Rev. Lett.* **112**, 147202 (2014).
- [35] A. K. Paul, M. Reehuis, V. Ksenofontov, B. Yan, A. Hoser, D. M. Többens, P. M. Abdala, P. Adler, M. Jansen, and C. Felser, Lattice Instability and Competing Spin Structures in the Double Perovskite Insulator Sr₂FeOsO₆, *Phys. Rev. Lett.* **111**, 167205 (2013).
- [36] A. K. Paul, A. Sarapulova, P. Adler, M. Reehuis, S. Kanungo, D. Mikhailova, W. Schnelle, Z. Hu, C. Kuo, V. Sirguri, S. Rayaprol, Y. Soo, B. Yan, C. Felser, K. H. Tjeng, and K. M. Jansen, Magnetically frustrated double perovskites: Synthesis, structural properties, and magnetic order of Sr₂BOsO₆ (B = Y, In, Sc), *Z. Anorg. Allg. Chem.* **641**, 197 (2015).
- [37] A. K. Paul, M. Jansen, B. Yan, C. Felser, M. Reehuis, and P. M. Abdala, Synthesis, crystal structure, and physical properties of Sr₂FeOsO₆, *Inorg. Chem.* **52**, 6713 (2013).
- [38] R. C. Williams, F. Xiao, I. O. Thomas, S. J. Clark, T. Lancaster, G. A. Cornish, S. J. Blundell, W. Hayes, A. K. Paul, C. Felser, and M. Jansen, Muon-spin relaxation study of the double perovskite insulators Sr₂BOsO₆ (B = Fe, Y, In), *J. Phys.: Condens. Matter* **28**, 076001 (2016).
- [39] A. K. Paul, M. Reehuis, C. Felser, P. M. Abdala, and M. Jansen, Synthesis, crystal structure, and properties of the ordered double perovskite Sr₂CoOsO₆, *Z. Anorg. Allg. Chem.* **639**, 2421 (2013).
- [40] P. Adler, V. Ksenofontov, A. K. Paul, M. Reehuis, B. Yan, M. Jansen, and C. Felser, Magnetic phase transitions and iron valence in the double perovskite Sr₂FeOsO₆, *Hyperfine Interact.* **226**, 289 (2014).
- [41] C. Felser and R. Seshadri, Conduction band polarization in some CMR materials: Evolving guidelines for new systems, *Int. J. Inorg. Mater.* **2**, 677 (2000).

- [42] J. M. Longo, P. M. Raccach, and J. B. Goodenough, Magnetic properties of SrRuO_3 and CaRuO_3 , *J. Appl. Phys.* **39**, 1327 (1968).
- [43] R. J. Cava, Schizophrenic electrons in ruthenium-based oxides, *Dalton Trans.* 2979 (2004).
- [44] A. Callaghan, C. W. Moeller, and R. Ward, Magnetic interactions in ternary ruthenium oxides, *Inorg. Chem.* **5**, 1572 (1966).
- [45] Y. Maeno, H. Hashimoto, K. Yoshida, S. Nishizaki, T. Fujita, J. G. Bednorz, and F. Lichtenberg, Superconductivity in a layered perovskite without copper, *Nature (London)* **372**, 532 (1994).
- [46] A. P. Mackenzie and Y. Maeno, The superconductivity of Sr_2RuO_4 and the physics of spin-triplet pairing, *Rev. Mod. Phys.* **75**, 657 (2003).
- [47] A. P. Mackenzie, J. A. N. Bruin, R. A. Borzi, A. W. Rost, and S. A. Grigera, Quantum criticality and the formation of a putative electronic liquid crystal in $\text{Sr}_3\text{Ru}_2\text{O}_7$, *Physica C* **481**, 207 (2012).
- [48] J. Chang, K. Lee, M. H. Jung, J.-H. Kwon, M. Kim, and S.-K. Kim, Emergence of room-temperature magnetic ordering in artificially fabricated ordered double-perovskite $\text{Sr}_2\text{FeRuO}_6$, *Chem. Mater.* **23**, 2693 (2011).
- [49] R. O. Bune, M. V. Lobanov, G. Popov, M. Greenblatt, C. E. Botez, P. W. Stephens, M. Croft, J. Hadermann, and G. V. Tendeloo, Crystal structure and properties of Ru-stoichiometric LaSrMnRuO_6 , *Chem. Mater.* **18**, 2611 (2006).
- [50] P. Kayser, B. Ranjbar, B. J. Kennedy, and M. Avdeev, The impact of chemical doping on the magnetic state of the Sr_2YRuO_6 double perovskite, *J. Solid State Chem.* **249**, 154 (2017).
- [51] P. M. Woodward, J. Goldberger, M. W. Stoltzfus, H. W. Eng, and R. A. Ricciardo, Electronic, magnetic, and structural properties of $\text{Sr}_2\text{MnRuO}_6$ and LaSrMnRuO_6 double perovskites, *J. Am. Ceram. Soc.* **91**, 1796 (2008).
- [52] P. D. Battle, T. C. Gibb, C. W. Jones, and F. Studer, Spin-glass behavior in $\text{Sr}_2\text{FeRuO}_6$ and BaLaNiRuO_6 : A comparison with antiferromagnetic BaLaZnRuO_6 , *J. Solid State Chem.* **78**, 281 (1989).
- [53] P. D. Battle, C. W. Jones, and F. Studer, The crystal and magnetic structures of $\text{Ca}_2\text{NdRuO}_6$, $\text{Ca}_2\text{HoRuO}_6$, and $\text{Sr}_2\text{ErRuO}_6$, *J. Solid State Chem.* **90**, 302 (1991).
- [54] C. Sakai, Y. Doi, Y. Hinatsu, and K. Ohoyama, Magnetic properties and neutron diffraction study of double perovskites $\text{Ca}_2\text{LnRuO}_6$ ($\text{Ln} = \text{Y}, \text{La-Lu}$), *J. Phys.: Condens. Matter* **17**, 7383 (2005).
- [55] E. Granado, J. W. Lynn, R. F. Jardim, and M. S. Torikachvili, Two-Dimensional Magnetic Correlations and Partial Long-Range Order in Geometrically Frustrated Sr_2YRuO_6 , *Phys. Rev. Lett.* **110**, 017202 (2013).
- [56] S. Tripathi, R. Rana, S. Kumar, P. Pandey, R. S. Singh, and D. S. Rana, Ferromagnetic CaRuO_3 , *Sci. Rep.* **4**, 3877 (2014).
- [57] H. T. Dang, J. Mravlje, A. Georges, and A. J. Millis, Electronic correlations, magnetism, and Hund's rule coupling in the ruthenium perovskites SrRuO_3 and CaRuO_3 , *Phys. Rev. B* **91**, 195149 (2015).
- [58] R. Mishra, J. R. Soliz, P. M. Woodward, and W. Windl, $\text{Ca}_2\text{MnRuO}_6$: Magnetic order arising from chemical chaos, *Chem. Mater.* **24**, 2757 (2012).
- [59] K. Nomura, R. Zboril, J. Tucek, W. Kosaka, S. Ohkoshi, and I. Felner, Substitution effects of barium and calcium on magnetic properties of $A_x\text{Sr}_{1-x}(\text{Fe}_{0.5}\text{Ru}_{0.5})\text{O}_3$ double perovskites ($x = 0.05$, $A = \text{Ba}, \text{Ca}$), *J. Appl. Phys.* **102**, 013907 (2007).
- [60] H. L. Feng, P. Adler, M. Reehuis, W. Schnelle, P. Pattison, A. Hoser, C. Felser, and M. Jansen, High-temperature ferrimagnetism with large coercivity and exchange bias in the partially ordered $3d/5d$ hexagonal perovskite $\text{Ba}_2\text{Fe}_{1.12}\text{Os}_{0.88}\text{O}_6$, *Chem. Mater.* **29**, 886 (2017).
- [61] I. A. Campbell and S. Senoussi, Re-entrant systems: A compromise between spin glass and ferromagnetic order, *Philos. Mag.* **65**, 1267 (1992).
- [62] R. A. Brand, H. Georges-Gibert, J. Hubsch, and J. A. Heller, Ferrimagnetic to spin glass transition in the mixed spinel $\text{Mg}_{1+r}\text{Fe}_{2-2r}\text{Ti}_r\text{O}_4$: A Mössbauer and DC susceptibility study, *J. Phys. F* **15**, 1987 (1985).
- [63] S. Chillal, M. Thede, F. J. Litterst, S. N. Gvasaliya, T. Shaplygina, S. G. Lushnikov, and A. Zheludev, Microscopic coexistence of antiferromagnetic and spin-glass states, *Phys. Rev. B* **87**, 220403(R) (2013).
- [64] S. Chillal, S. N. Gvasaliya, A. Zheludev, D. Schroeter, M. Kraken, F. J. Litterst, T. A. Shaplygina, and S. G. Lushnikov, Magnetic short- and long-range order in $\text{PbFe}_{0.5}\text{Ta}_{0.5}\text{O}_3$, *Phys. Rev. B* **89**, 174418 (2014).
- [65] W. Kleemann, V. V. Shvartsman, P. Borisov, and A. Kania, Coexistence of Antiferromagnetic and Spin Cluster Glass Order in the Magnetoelectric Relaxor Multiferroic $\text{PbFe}_{0.5}\text{Nb}_{0.5}\text{O}_3$, *Phys. Rev. Lett* **105**, 257202 (2010).
- [66] L. Shlyk, B. Strobel, B. Farmer, L. E. De Long, and R. Niewa, Coexistence of ferromagnetism and unconventional spin-glass freezing in the site disordered kagome ferrite $\text{SrSn}_2\text{Fe}_4\text{O}_{11}$, *Phys. Rev. B* **97**, 054426 (2018).
- [67] G. Cao, J. Zhang, S. Wang, J. Yu, C. Jing, S. Cao, and X. Shen, Reentrant spin glass behavior in CE-type AFM $\text{Pr}_{0.5}\text{Ca}_{0.5}\text{MnO}_3$ manganite, *J. Magn. Magn. Mater.* **301**, 147 (2006).
- [68] J. Rodríguez-Carvajal, Recent advances in magnetic structure determination by neutron powder diffraction, *Physica B* **192**, 55 (1993).
- [69] V. F. Sears, in *International Tables for Crystallography*, edited by A. J. C. Wilson (Kluwer, Dordrecht, 1995), Vol. C, p. 383.
- [70] P. J. Brown, in *International Tables for Crystallography*, edited by A. J. C. Wilson (Kluwer, Dordrecht, 1995), Vol. C, p. 391.
- [71] Z. Klencsár, A. Kuzmann, and A. Vértés, User-friendly software for Mössbauer spectrum analysis, *J. Radioanal. Nucl. Chem.* **210**, 105 (1996).
- [72] See Supplemental Material at <http://link.aps.org/supplemental/10.1103/PhysRevB.98.224423> for further structural, Mössbauer, and transport data.
- [73] E. F. Bertaut, Representation analysis of magnetic structures, *Acta Cryst. A* **24**, 217 (1968).
- [74] M. Reehuis, C. Ulrich, P. Pattison, B. Ouladdiaf, M. C. Rheinstädter, M. Ohl, L. P. Regnault, M. Miyasaka, Y. Tokura, and B. Keimer, Neutron diffraction study of YVO_3 , NdVO_3 , and TbVO_3 , *Phys. Rev. B* **73**, 094440 (2006).
- [75] P. M. Woodward, D. E. Cox, E. Moshopoulou, A. W. Sleight, and S. Morimoto, Structural studies of charge disproportionation and magnetic order in CaFeO_3 , *Phys. Rev. B* **62**, 844 (2000).
- [76] M. Schmidt, M. Hofmann, and S. J. Campbell, Magnetic structure of strontium ferrite $\text{Sr}_4\text{Fe}_4\text{O}_{11}$, *J. Phys. Condens. Matter* **15**, 8691 (2003).

- [77] P. Kayser, S. Injac, B. Ranjbar, B. J. Kennedy, M. Avdeev, and K. Yamaura, Magnetic and structural studies of Sc containing ruthenate double perovskites $A_2\text{ScRuO}_6$ ($A = \text{Ba}, \text{Sr}$), *Inorg. Chem.* **56**, 9009 (2017).
- [78] K. Binder and A. P. Young, Spin glasses: Experimental facts, theoretical concepts, and open questions, *Rev. Mod. Phys.* **58**, 801 (1986).
- [79] J. A. Mydosh, *Spin Glasses: An Experimental Introduction* (Taylor & Francis, London, 1993), p. 256.
- [80] J. Lago, S. J. Blundell, A. Eguia, M. Jansen, and T. Rojo, Three-dimensional Heisenberg spin-glass behavior in $\text{SrFe}_{0.90}\text{Co}_{0.10}\text{O}_{3.0}$, *Phys. Rev. B* **86**, 064412 (2012).
- [81] A. Malinowski, V. L. Bezusyy, R. Minikayev, P. Dziawa, Y. Syryanny, and M. Sawicki, Spin-glass behavior in Ni-doped $\text{La}_{1.85}\text{Sr}_{0.15}\text{CuO}_4$, *Phys. Rev. B* **84**, 024409 (2011).
- [82] P. Bag, P. R. Baral, and R. Nath, Cluster spin-glass behavior and memory effect in $\text{Cr}_{0.5}\text{Fe}_{0.5}\text{Ga}$, *Phys. Rev. B* **98**, 144436 (2018).
- [83] N. F. Mott and E. A. Davis, *Electronic Processes in Non-Crystalline Materials* (Clarendon, Oxford, 1979).
- [84] N. F. Mott, Conduction in non-crystalline materials, *Philos. Mag.* **19**, 835 (1969).
- [85] L. Zhang and Z. J. Tang, Polaron relaxation and variable-range-hopping conductivity in the giant-dielectric-constant material $\text{CaCu}_3\text{Ti}_4\text{O}_{12}$, *Phys. Rev. B* **70**, 174306 (2004).
- [86] S. K. Deshpande, S. N. Achary, R. Mani, J. Gopalakrishnan, and A. K. Tyagi, Low-temperature polaronic relaxations with variable range hopping conductivity in FeTiMO_6 ($M = \text{Ta}, \text{Nb}, \text{Sb}$), *Phys. Rev. B* **84**, 064301 (2011).
- [87] G. Popov, M. Greenblatt, and M. Croft, Large effects of A-site average cation size on the properties of the double perovskites $\text{Ba}_{2-x}\text{Sr}_x\text{MnReO}_6$: A d^5-d^1 system, *Phys. Rev. B* **67**, 024406 (2003).
- [88] L. S. I. Veiga, G. Fabbris, M. van Veenendaal, N. M. Souza-Neto, H. L. Feng, K. Yamaura, and D. Haskel, Fragility of ferromagnetic double exchange interactions and pressure tuning of magnetism in $3d-5d$ double perovskite $\text{Sr}_2\text{FeOsO}_6$, *Phys. Rev. B* **91**, 235135 (2015).
- [89] Y. S. Hou, H. J. Xiang, and X. G. Gong, Lattice-distortion induced magnetic transition from low-temperature antiferromagnetism to high-temperature ferrimagnetism in double perovskites $A_2\text{FeOsO}_6$ ($A = \text{Ca}, \text{Sr}$), *Sci. Rep.* **5**, 13159 (2015).
- [90] T. C. Gibb, A study of superexchange interactions in the perovskite $\text{Sr}_2\text{FeRuO}_6$ by Monte Carlo analysis, *J. Mater. Chem.* **15**, 4015 (2005).
- [91] S. N. Kaul, V. Siruguri, and G. Chandra, Magnetization and Mössbauer study of the reentrant amorphous $\text{Fe}_{90}\text{Zr}_{10}$ alloy, *Phys. Rev. B* **45**, 12343 (1992).
- [92] I. A. Campbell, S. Senoussi, F. Varret, J. Teillet, and A. Hamzić, Competing Ferromagnetic and Spin-Glass Order in a AuFe alloy, *Phys. Rev. Lett.* **50**, 1615 (1983).